We are grateful to the referee #1 and referee #2 for the valuable comments, which helped us to further improve our manuscript. Below we address the reviewer's comments, with reviewer comments are in black and our answers are in purple.

Before we provide the detailed point to point reply, we provide an overview of main changes and improvements:

1. A new figure and a new Table are included (see Fig. 2 and Table 4 in the revised manuscript) to evaluate the meteorological conditions, and these are discussed in the beginning of the results part. It shows that the WRF-Chem performed well in simulating the meteorological conditions during our simulation period. So, the differences of simulated dust emission and deposition are attributed to the different emission and dry deposition schemes.
2. We examined how the daily AOD evolves during the whole dust event period in Fig. 9. The time evolution of the dust storm is helpful to better quantify which dust emission scheme work better for this case, as this will further help to quantify which dry deposition schemes works better. Compared with daily MODIS AOD (Fig. 9), our results indicate that dust emission from Shao2011 is better for this dust event, in terms of dust spatial and temporal distributions. We can then conclude that Z01 dry deposition scheme performs the best among three dry deposition schemes we evaluated (Fig. 8).
3. The vertical extinction coefficient profile from CALIPSO is used to evaluate the vertical dust distribution (Fig.10).
4. We added more description for the important terms like "rebound effect," "collection efficiency from interception, "collection efficiency from impaction " to help readers understand why differences in these parameters matter for the dry deposition process (Sect. 2.3).

Referee #1

Interactive comment on "WRF-Chem v3.9 simulations of the East Asian dust storm in May 2017: modeling sensitivities to dust emission and dry deposition schemes" by Yi Zeng et al.

Sagar Parajuli (Referee)
psagar@utexas.edu

Received and published: 15 December 2019

Detailed Review: The paper is mostly well written and well structured. The main scientific value of the paper is that it helps to identify the best depositional scheme for WRF Chem model. However, the model simulations were performed over a short period so the conclusions are questionable.

Thank you for the comments. As the main purpose of this paper is to highlight the importance of the dry deposition process that is often overlooked in dust transport models, even with a short time period dust storm simulation, we still can see the large dust loading difference which is attributed to the dry deposition scheme. What is more, we further evaluated simulated meteorological fields and found that simulated fields are close to those from the reanalysis fields and that different experiments produce very similar meteorological fields in the revised manuscript. This partly alleviates the limitation of the short-term simulation. We do acknowledge the potential limitation of the simulation over a short period, and longer simulations are desirable in the future to test whether the optimal scheme here still produces best simulations. This is now also added in Sect. 4.

1. Line 215: cite the figure that shows the study domain.

Thank you for the suggestion. Now we expanded Fig.4 to show the study domain and changed it to Fig.1. And we also cited the Fig.1 in Sect. 2.4 (P11 L253).

2. 219: You say here: The meteorological conditions are reinitialized every 24 hours. But then you say only chemical conditions are reinitialized. Which one is true? Please specify the details explaining how exactly you implemented this in WRF Chem and which variables you updated.

Thanks. The meteorological conditions are reinitialized but the chemistry not reinitialized. For meteorological conditions (such as wind speed and temperature), we reinitialized every 24 hours using NCEP/FNL reanalysis data. For chemistry, the output of the aerosol field (such as the concentration of different aerosol species) from the previous 1-day run was used as the initial chemical conditions for the next 1-day run. Our simulation period is from 26 April to 7 May 2017. So one experiment consists of 12 one-day runs. For each one-day run, the NCEP/FNL data is used as initial meteorological condition, and the chemistry is from the last time step of the last one-day run. This can be achieved by setting chem_in_opt=1 in namelist.input. In this way, the chemical field are continuous and we can also get more reliable

meteorological conditions. We also specify the details in the main text (P12 L259-263).

3. MOSAIC 8 bin scheme is computationally intensive and it is understandable why the authors chose 4 bin option. But I don't understand why you conducted simulations only for a dust episode (1week). Whenever one intends to evaluate a model, he/she must design the experiment more consciously. A year-long simulation is ideal because seasonal aspect has to be covered. This could be achieved by increasing the resolution or reducing the size of the domain. Of course, we must find a balanced model set up that serves to investigate our research goal.

Thank you for the comments. Please also see our reply to general comment from reviewer #1. As the main purpose of this paper is to highlight the importance of the dry deposition process that is often overlooked in dust transport models, even with a short time period dust storm simulation, we still can see the large dust loading difference which is attributed to the dry deposition scheme. What is more, we further evaluated simulated meteorological fields and found that simulated fields are close to those from the reanalysis fields and that different experiments produce very similar meteorological fields in the revised manuscript. This partly alleviates the limitation of the short-term simulation. Because we simulated the complete processes of a typical spring dust event in East Asia, it also has certain value for the prediction and simulation of dust storm cases in East Asia. We do acknowledge the potential limitation of the simulation over a short period, and longer simulations are desirable in the future to test whether the optimal scheme here still produces best simulations. This is now also added in Sect. 4.

4. 245-285: These results are just some comparison and are not of much scientific value. There are several other previous studies which have compared different dust emission schemes. You have compared the simulated AOD with MODIS AOD which is good enough. Dust depositional aspect is not covered in the literature much so I suggest the authors to stick to the depositional aspect on this paper. I don't see why it was necessary to conduct simulations with different dust schemes because the main purpose of the study was to investigate the dry deposition processes.

Thanks for your comments! The main purpose of this study is to study the sensitivity of dust simulation to dry deposition schemes, and the performance of different dry deposition schemes. Here are two reasons why we also want to evaluate dust

emission scheme. One is that although there have been several previous studies comparing different dust emission schemes (Kang et al., 2011; Su and Fung, 2015; Wu and Lin, 2014; Yuan et al., 2019), their studies are all under the framework of the GOCART aerosol scheme. The dry deposition treatment of GOCART aerosol scheme seems to have big problems for dust simulation (Zhang et al., 2019). And the size distribution of the emitted dust is also different between the GOCART and MOSAIC aerosol scheme. So we do not know yet which dust emission scheme is best for our dust storm simulation based on the previous studies. Another reason is that in the currently released version of WRF Chem, only GOCART dust emission scheme is coupled in MOSAIC aerosol scheme. As shown in our manuscript, the GOCART dust scheme strongly underestimated dust concentrations in comparison with observations, no matter which dry deposition scheme we used. Therefore, we have newly implemented the Shao2011 scheme into MOSAIC aerosol scheme. If we put the results of Shao2011 directly, the readers may wonder why we don't use the default scheme and make large efforts to implement a new one. If no comparison of these two dust emission schemes is included in our manuscript, readers may feel confused. Therefore, we also briefly compare the differences between the two widely used dust emission schemes, which can provide a reference for readers who want to use the MOSAIC aerosol scheme to simulate dust storm in the future. Please also see our reply to specific comment # 4 from reviewer #2.

5. 200: It might be wise to define rebound effect, interception and collection efficiency in a simple, understandable language for the benefit of readers. Coming to the world of 'reality' from the world of 'equations' and giving some practical definition would be good. What happens when the dust falls on the leaves or a surface? What is the effect of type/condition of surface on dust deposition? Wet surface or dry surface, does it matter? And what happens after deposition? Does the deposited dust get blown away, or does it get washed away? Are these equations of depositions considering realistic processes? Or Are they just some 'theoretical' equations?

We added the description for rebound effect in Sect. 2.3 and it reads "When large particles (usually >5 μm) hit the non-sticky surface, they are liable to rebound from the surface if they have sufficient kinetic energy. The rebound factor R represents the fraction of particles that stick to the surface." (P11 L242-244)
We added the description for collection efficiency from interception in Sect. 2.3.3 and it reads "E_{IN} is the collection efficiency based on the relative dimensions of the

particle to the collector diameter (Gallagher, 2002). Interception occurs when particles moving with the mean flow and the distance between an obstacle and particle center is less than half of the diameter. Then the particles will collide with and be collected by the obstacle" (P10 L228-231)
We added the description for collection efficiency from impaction in Sect. 2.3.1 and it reads "E_{IM} is the collection efficiency due to impaction of the particle with the collecting surface (Gallagher, 2002). Impaction occurs when there are changes in the direction of airflow, and particles that cannot follow the flow will collide with the obstacle and stay on the surface due to the inertia (Giardina and Buffa, 2018)." (P9 L194-196)

6. 232: . . ..stations. . .please mention "locations shown in results section".

Improved. (P13 L277)

7. 403-404: On what basis? Based on Table 4? Please refer to the correlation/rmse values and discuss.

We added the correlation/rmse values and discussed (P22 L506-509). It reads "For PM10, S11Z01 experiment gives the largest R of 0.83 and the smallest RMSE of 82.98 of all the stations (Table 5). The spatial distribution of AOD during the simulation period obtained by S11Z01 is closet to MODIS AOD (Fig. 9), with the largest R and a relatively small RMSE (Table 6)."

8. 845: Figure 6, you mentioned that 1000 stations data were used but in the figure, it appears that most stations lie outside the six boxes chosen. Why not use all the stations?

In Fig8 (Fig. 7 in the original manuscript), we want to analyze the performance of different experiments in different regions. So we divided the domain into five subregions, with two dust source regions and three remote regions that is largely affected by this dust storm. We did calculate the R and RMSE for all the stations in Table 5 (see the last row of Table 5). We note that the total is not for all the stations of the subregions but for all the stations over the whole China that we showed in Fig. 7 (more than 1000 stations), and this is now clarified in the header of Table 5 (P37 L842).

9. 850 Figure 7: Are the statistics calculated using daily-mean data? Please mention about this in the Figure caption.

Thanks. We used time-averaged PM10 data over 1-7 May. We also added this in the Figure 8 caption (P49 986-987).

10. Line 368-373: The study domain is big and there exist time differences in different areas. How did you extract output at 13:00pm local time? If you are using level-3 MODIS data, using daily-average data would be fine because 1:30 pm local time is only at equator.

First, we divided the domain into different time zones according to the longitude. Then we can get the UTC when the local time is 13:00 in different time zones. Next, the simulated AOD results are extracted at the corresponding UTC to build an AOD map for the entire domain for each day. Finally, these processed daily model results are compared with the MODIS daily AOD data. For example, for the UTC+8 Time Zone with longitude near 120E, we use the WRF-Chem simulated AOD at 05:00 UTC to compare with the MODIS daily AOD data.
Yes, we are using the level-3 MODIS data. As the A-Train satellites pass most region of Earth at around 13:30 local time, we think it would be more reasonable to use the model results at 13:00 local time in each region to compare with MODIS daily AOD data.
We also revised our description of the comparison method to make it clear in Sect. 2.5.2. It reads “For the model results, first we divided the domain into different time zones according to the longitude. Then the model results at corresponding UTC when the local time is 13:00 are extracted. The collocated model AOD results for each day are used to compared with daily MODIS AOD.” (P13 L289-292)

11. Figure8, the shaded color appears only in northern China region and data look empty in most region. Why so much data gaps in the model results? And why only use the data for May 7? My suggestion is to use time-averaged AOD during the dust episode and do the comparison.

As for data gaps in the model results, this is because the model results are already collocated with MODIS observation. Grid points without valid MODIS AOD retrieval are masked for both observational and model results in Fig. 9. In this way, it is more intuitive to see which experiment is closer to MODIS AOD. This question is

mentioned in the caption of Fig. 9 (P50 L1003-1004). We also describe this in the main text. (P20 L458-459)

For the second question, as we also want to show the different stages of this dust storm (e.g. dust emission and dust transport), we now plot the AOD at 13:00 local time during this episode from 1-5 May (Fig.9). And the description has been updated accordingly (P20 L459-470).

12. 380-384: Low correlation is understandable because WRF Chem can't reproduce dust events at hourly or daily time scale. It is extremely challenging to model short-lived dust events. So don't blame it to MODIS data. But, it would be better to time-average the data during the whole period (1-7may) and calculate spatial correlation coefficient and corresponding RMSE. Were R and RMSE calculate in this manner?

Thanks. The R and RMSE are indeed calculated during the whole period (1-7 May) in Table 6 (Table 5 in the original manuscript). For each day, we just use the results at 13:00 local time for each region. Then we averaged the model results at 13:00 of the 7 days and compared them with MODIS 7-day average. Please see our reply to comment #10 from reviewer #1 for the detail calculation.

Referee #2

Interactive comment on "WRF-Chem v3.9 simulations of the East Asian dust storm in May 2017: modeling sensitivities to dust emission and dry deposition schemes" by Yi Zeng et al.

Sandra LeGrand (Referee)
sandra.l.legrand@usace.army.mil

Received and published: 19 December 2019

General Comments:

This study presents an investigation of dust simulation sensitivity to three dry dust deposition schemes and two adaptations of widely used dust emission schemes using the Weather Research and Forecasting model coupled with chemistry (WRF-Chem). The authors successfully demonstrate that airborne dust concentration and transport simulation can be sensitive to dry deposition process parameterization. Moreover,

their findings make a compelling case that future efforts should focus on improving dry dust deposition schemes (in addition to dust emission schemes) and that more field measurements of dry deposition are needed to reduce uncertainties in dust simulation. The authors did a good job introducing and comparing the deposition scheme physics in section 2.3 and should be commended for finding/reporting several undocumented discrepancies in the various WRF-Chem model versions. Overall, this paper brings attention to a process that is often overlooked in dust transport model assessment and is of value to the modeling community.

1. However, critical gaps remain in the authors' methodology that need to be addressed before publication moves forward. The current approach supports the authors' assessment that GOCART and Shao2011 produce markedly different dust emission flux patterns, BS95 removed the most dust from the atmosphere, Z01 removed the least dust from the atmosphere, and the S11Z01 combination produced the best simulation of average PM10 and AOD for this case study. These results, however, may only be applicable to this case study and particular WRF-Chem configuration.

For example, the authors did not include or allude to an analysis of how well the model simulated the general meteorological conditions driving the dust events. How well did the model winds (surface and aloft), synoptic conditions, etc. verify against observations? This is a necessary step to be able to discern whether simulation outcomes (good or bad) are actually due to dust scheme physics or an artifact of erroneous forcing conditions.

Many thanks for your comments and constructive suggestions! We agreed it is indeed important to evaluate how well the general meteorological conditions are simulated for a study based on a dust storm event. We now added the evaluation of the meteorological conditions in the revised manuscript. A new figure and a new Table are included (see Fig. 2 and Table 4 in the revised manuscript), and these are discussed in in the beginning of the results part (Sect. 3. 1 P14 L304-324). It shows that the WRF-Chem performed well in simulating the meteorological conditions during our simulation period. So, the differences of simulated dust emission and deposition are attributed to the different emission and dry deposition schemes. Through the evaluation of the meteorological conditions, we have a deeper understanding of the dominant weather system for the dust emission processes, and

this help us to identify which dust emission scheme correctly captured the emission phase of this dust event (see our reply below).

2. Also, it is unclear which dust emission scheme correctly captured the emission phase se of this dust event (with respect to magnitude, spatial footprint, and temporal patterns). Assuming the Taklimakan and Gobi Deserts are the primary sources of dust, the scatter plots from Figure 7 seem to indicate GOCART did a better job with dust emission from the Taklimakan Desert and that there's little difference between the results of the two dust emission schemes for the Gobi Desert region. Figure 2 shows maps of the total simulated dust loading from the two dust emission schemes. GOCART clearly produces widespread low-level dust emission, while Shao2011 emits stronger dust plumes from localized sources, mostly from the Gobi Desert region. The AOD comparison in Figure 8 is for midway through the dust event. It is unclear if dust originated in the Taklimakan Desert and was transported, if the Taklimakan Desert region in the AOD observation is cloud obscured, or if the dust in the Gobi Desert is entirely local.
Furthermore, because the authors have chosen to evaluate the dust emission and deposition schemes simultaneously, it's difficult to draw more generalizable conclusions about deposition scheme performance. Z01 may appear to be the best dry deposition scheme, but the slower deposition rate in Z01 may be compensating for the dust emission schemes not producing enough dust in the first place, issues with boundary layer mixing, or simulated winds that were too weak.

Many thanks for the comments and constructive suggestions! We agree it is indeed helpful to better quantify which dust emission schemes may work better for this case, as this will further help to quantify which dry deposition schemes works better. One way for better quantifying how well dust emissions are simulated is to examine how dust emission phase is simulated as the reviewer suggested. We now examined how the daily AOD evolves during the whole dust event period in Fig. 9. The upper panel of Fig. 9 shows the MODIS daily AOD from 1 May to 5 May. We can see relatively small dust emission in the GD on 1 May (Fig. 9a), and the emitted dust is transported eastward on 2 May (Fig. 9b). The main dust emission of this dust storm occurred on 3 May (Fig. 9c), and the dust emission over the GD is really large. Meanwhile, the newly added Fig.S1c and Fig. 2c shows that the Mongolian cyclone on 3 May developed vigorously and caused the large wind speed over the GD. At this stage, the TD has only very small dust emission. Along with the southeast wind and the northeast wind (Fig. S1c, S1e and Fig. 2c, 2e), the dust emission from the GD

(Fig.9c) was transported to the northeast and southeast of China (Fig. 9d). The TD has a very small amount of dust emission, and its contribution to this dust storm is small. Overall, our results indicate that this dust storm is mainly caused by the huge dust emission from the GD.

Figure 9 shows that Shao2011 well simulated the dust emission process over the GD on 3 May (Fig. 9m), while GOCART obviously underestimated the dust emission over the GD (Fig.9h). Though Fig. 8 (Fig. 7 in the original manuscript) indeed shows that GOCART is better than Shao2011 over the TD region, the dust emission over the TD is very small, and the dust over TD is not easily transported to northeast and Southeast China due to terrain and meteorological conditions.

We also can see that the main dust source regions over the GD are located in the westernmost of Inner Mongolia Province and the southernmost of Mongolia (Fig. 9c). However, from the PM10 observational sites plot (Fig. 7), we can see that in the westernmost of Inner Mongolia Province and the southernmost of Mongolia, there is almost no PM10 observational site. So from the scatter plot (Fig. 8), there is little difference between the results of the two dust emission schemes for the GD. However, away from the dust source region (Fig. 7, NCP,NEP and YR), Shao2011 is significantly better than GOCART.

Overall, our results indicate that dust emission from Shao2011 is better for this dust event, in terms of dust spatial and temporal distributions. Based on the Shao2011 dust emission scheme, we can then comfortably conclude that Z01 dry deposition scheme performs the best among three dry deposition schemes we evaluated (Fig. 8d,8e,8f). Moreover, even with the GOCART scheme, Figure 8 also showed that Z01 performs the best.

We now incorporate these discussions in the revised manuscript (Sect. 3.4 and Sect. 4).

3. An overview of how well the model (or each simulation depending on whether or not aerosol feedbacks were affecting weather evolution) captured the general atmospheric conditions of the case study event is needed. This could be part of the main text or added as an appendix. This is particularly important given the strong influence of wind flow/turbulence and boundary layer mixing on the deposition process.

Thanks for the suggestion. The evaluation of the meteorological conditions is now added. See our reply above (general comment #1 from reviewer #2).

4. Dust emission observations are difficult to obtain (or in some cases non-existent). Understanding the evolution of the weather forcing conditions in combination with the dust emission simulation results, and possibly even qualitative assessment of true or false color satellite imagery, would enable the authors to make inferences as to which dust emission treatment was more accurate for this particular case study. Timeseries plots comparing PM10 observations to simulated PM10 values from grid points in/near the source regions may also offer some insight.

Thanks for the suggestion! We now indeed include the time evolution of simulated AOD and compare them with MODIS observations. This helped us to identify which dust emission scheme is better in simulating this dust event. See our reply above (general comment #2 from reviewer #2).

5. Given the focus on deposition, this paper really should include an assessment of the simulated vertical dust distribution. For example, the authors could add a comparison of simulated vertical dust distribution to CALIOP LiDAR observations from the CALIPSO satellite (Winkler, 2009; available via the NASA Earth Data Portal at https://search.earthdata.nasa.gov/) in order to demonstrate that simulated dust was in good agreement with observed plume heights before making assumptions about fall rate accuracy.

Thank you for the suggestion. We now added a new figure (Fig.10) to evaluate the vertical dust distribution. The extinction coefficient from CALIPSO is used. We added the description of CALIPSO data (P13 L293-301) and the extinction coefficient evaluation (P21 L477-485). All the six experiments show the similar dust location in the atmosphere, which is consistent with the CALIPSO observation. The simulated extinction coefficients using GOCART dust emission schemes are significantly underestimated compared to the CALIPSO observation (Fig. 10a,10b and 10c), while the modeled vertical extinction coefficients using Shao2011 dust emission scheme agrees better with observation though they are still underestimated (Fig. 10e,10f and 10g). Among all the six experiments, results from S11Z01 agree the best with observation (Fig. 10).

Hopefully, these issues can be easily addressed with additional plots and documentation. Papers by Ma et al. (2019), Letcher and LeGrand (2018), Rizza et al. (2017), and Nguyen et al. (2019) offer good examples of approaches for general dust

case study descriptions, forcing weather evaluations, and/or vertical dust distribution assessments.

Many thanks for your constructive comments and suggestions. Following your suggestions and these papers, we now added new analysis of the meteorological conditions and the time evolution of the dust storm. We believe these new analyses have greatly improved the manuscript. Please see our detailed reply above.

Specific Comments:

1. P3 L59: "Large-size" is a relative term. Please provide a value for a frame of reference. For example, ". . . large-size aerosol particles (e.g., diameters > X μm), such as dust."

We added the reference value for the large-size aerosol particles **(eg., diameters > 2.5 μm)** (P3 L60).

2. P3 L69, P13 L282, P17 L398, P18 L401: "A lot" is somewhat colloquial for use in an academic paper.

Thanks. We changed our expressions to make it more academic accordingly. Below we list our modifications:

(1) "the dust emission fluxes and surface concentrations **differ a lot**." has been replaced by "**significant difference exist** in the dust emission fluxes and surface concentrations" (P3 L70-71)

(2) "Simulated dust emission fluxes can **differ a lot** between two versions of the Shao2011 scheme" has been replaced by "simulated dust emission fluxes **are quite different** when using two versions of the Shao2011 scheme" (P16 L368).

(3) "as dust emission fluxes in dust source regions **differ a lot** among different dust emission schemes" has been replaced by "as dust emission fluxes in dust source regions **differ substantially** among different dust emission schemes" (P22 L500)

(4) "and simulated dust emission fluxes between WRF-Chem v3.9 and WRF-Chem v3.7.1 can **differ a lot**" has been replaced by "and **significant difference exist in** the simulated dust emission fluxes between WRF-Chem v3.9 and WRF-Chem v3.7.1" (P22 L502-503).

3. P3 L71: Please adjust the text to make it clear that the papers by Yuan et al. (2019) and Chen et al. (2017) are also WRF-Chem studies.

We added "…WRF-Chem simulation of …" to make it clear that the paper by (Yuan et al., 2019) is WRF-Chem study (P4 L75). And we also added "In another WRF-Chem study…" to make it clear that the paper by (Chen et al., 2017a) is WRF-Chem study (P4 L77-79).

4. P4 L75: Why is it important to evaluate the dust emission and deposition schemes simultaneously? Wouldn't it be better to select a case study with well-simulated dust emissions from a single dust emission scheme when assessing model sensitivity to deposition scheme configuration? Model performance assessment for different pairings of dust emission and deposition schemes over an extended period of time may be of value to some readers, but evaluating the two aspects of the dust transport process simultaneously for a single case study event introduces extra degrees of freedom that make it difficult to ascribe model performance to a particular root cause.

Thanks for your comments. As we mentioned in our reply to comment #4 from reviewer#1, there are two reasons why we also evaluated dust emission schemes in our manuscript. One is that although there have been several previous studies comparing different dust emission schemes, these studies are all under the framework of the GOCART aerosol scheme, but the dry deposition treatment of GOCART aerosol scheme is problematic for dust simulation based on Zhang et al. (2019). So we do not know yet which dust emission schemes is best for our dust storm simulation based on the previous studies. The other reason is that in the currently released version of WRF Chem, only GOCART dust emission scheme is coupled in MOSAIC aerosol scheme. As shown in our manuscript, the GOCART dust scheme strongly underestimated dust concentrations in comparison with observations, no matter which dry deposition scheme is used. Therefore, we have newly implemented the Shao2011 scheme into MOSAIC aerosol scheme. In the revised manuscript, we also followed the suggestion from the reviewer to examine the evolution of simulated AOD in comparison with MODIS observation for the period of 1-5 May. In combination with the evaluations of meteorological conditions and other aspects of dust simulations, we now can see that Shao2011 indeed performs better for simulating this dust event (see also our reply to general comment #2 from reviewer #2). We believe this comparison therefore indeed

provide new knowledge to the field and provides a good reference for the community.

5. P4 L82-84: The authors reference a study by Zhang et al. (2019) that found that the WRF-Chem GOCART model underestimated dry deposition in north-west China by more than an order of magnitude compared to observations. Interestingly, the study by Zhang et al. (2019) was done using WRF-Chem v3.7.1. An error was recently discovered in how the GOCART gravitational settling code was implemented in WRF-Chem that also affects the calculation of the dry deposition rate (see code commit change comment in the WRF source code repository by Alexander Ukhov; https://github.com/openwfm/WRF-Fire-merge/commit/2ffdebf4ac311a5b1ef8cd0c639e0d857b550fdb). Given that this error wasn't corrected until the release of WRF-Chem v4.1, the findings from Zhang et al. (2019) may no longer be representative of GOCART in the current WRF-Chem release. It would be good if the authors note that here for reader awareness.

Thank you very much for the important information. We read the bug fix in GOCART gravitational settling carefully. Before the bug fix, the dust mass is not balanced, with deposited dust and dust in the atmosphere > emitted dust, because there is incorrect dust mass increasing in the gravitational settling subroutine. After the bug fix, the dust mass is balanced, with deposited dust and dust in the atmosphere = emitted dust, which leads to even lower dust deposition after the bug fix compared to that before the bug fix. So after the bug fix, the conclusion from Zhang et al. (2019) that "WRF-Chem GOCART model underestimated dry deposition in north-west China by more than an order of magnitude compared to observations" still holds and the underestimation of dust deposition in WRF-Chem becomes even larger.

6. P5 L101: "The model setups are listed. . ." wording is odd. Suggest changing to "A summary of the settings used to configure the model are listed. . ."

Thanks! This is now updated (P5 L106-107).

7. P5 L103 and Table 1 – Please add the radiation time step to your model description. Simulated wind speeds and dust emission flux appear to be very sensitive to this parameter when using RRTMG (not well documented). Also, please include the land

use dataset (lu_index) used for this study in the configuration description given that some of the deposition scheme parameters have dependencies on land use categories.

Thank you for your suggestion. We added the radiation timestep (radt) in the Sect. 2.4 (P12 L255). We added the land category (num_land_cat) in Table1. And we also added the descriptions of land category in Sect. 2.1 (P5 L108-109).

8. P5 L107-109: Suggest combining the following sentences to avoid redundancy: "The MOSAIC aerosol scheme uses sectional approach to represent aerosol size distribution. The MOSAIC 4-bin aerosol scheme divides aerosol particles into four size bins by aerosol diameter: 0.039-0.156, 0.156-0.625, 0.625-2.5, 2.5-10.0 μm." Suggest changing to: "The MOSAIC 4-bin aerosol scheme divides airborne particles into four size bins by their effective diameter (0.039-0.156, 0.156-0.625,0.625-2.5, 2.5-10.0 μm) to represent aerosol size distribution."

Thanks for the suggestion. We combined the two sentences to one accordingly (P5 L114-117).

9. P5 L112: Suggest deleting "from dust emission schemes" to avoid redundancy.

Thanks! This is now removed (P5 L121).

10. P6 L122-123: This statement as written (also stated in other peer-reviewed publications) misrepresents the findings from the Shao et al. (2011) paper. Shao et al. (2011) concluded that their simplified scheme produced similar results to the Shao (2004) scheme when compared to observations from the Japan-Australian Dust Experiment (JADE). The same Shao et al. (2011) paper also notes that these findings shouldn't be generalized due to the conditions of the JADE experiment. Recommend the authors simply note that they chose to use the most simplified version of the University of Cologne (UoC) dust emission schemes for their experiment or confirm Shao2004 and Shao2011 produce similar dust emission flux outcomes for their particular case study.

Thanks. We removed the sentence "but the performances of the full scheme (Shao2004) and the simplified scheme are equally effective (Shao et al., 2011)". (P6 L134-136) As we didn't perform the simulation of Shao2004, we just simply note that

we choose to use the most simplified version of the UoC dust emission scheme (P6 L137-140).

11. P6 Section 2.2.1: The GOCART emission scheme description is rather sparse compared to the Shao scheme descriptions. The authors reference the paper on MOSAIC by Zhao et al. (2010), which offers a similar brief overview of the GOCART dust emission scheme and references the original Ginoux et al. (2001) paper. However, closer examination of the code (subroutine mosaic_source_du in module_mosaic_addemiss.F) indicates dust_opt=13 (at least in v3.9) also includes the modifications to the original GOCART dust emission scheme (dust_opt=1) documented by LeGrand et al. (2019; Section 3.2.1) with the exception of the C parameter (default C value is set to 1 ×10−9 kg s2 m−5 consistent with the original Ginoux et al. (2001) paper). It would be good if the authors could expand this section given the general lack of documentation on the WRF-Chem dust_opt=13 setting (currently not included in the WRF-Chem user's manual). Also, the paper by Zhao et al. (2010) explored more than one modal size distribution configuration. It would be beneficial to readers for the authors to describe how the emitted dust particle size distribution used in dust_opt=13 is prescribed.

Thank you for the suggestion. Now we add the description of the dust_opt=13 in detail in Sect. 2.2.1. We added the description of size distribution for dust_opt=13 in Sect 2.2.1. It reads "The original GOCART dust emission scheme in GOCART aerosol scheme (dust_opt=1) calculates the dust emission flux from 0.2 to 20 μm. For GOCART dust scheme in MOSAIC aerosol scheme (dust_opt=13), the total dust emissions from 0.2 to 20 μm are redistributed to the size bins of MOSAIC (0.039-0.156, 0.156-0.625, 0.625-2.5 and 2.5-10.0 μm) with mass fractions of 0%, 0.38%, 8.8%, 68.0%". (P7 L152-155)
And we note here that in addition to the size distribution, the values of empirical proportionality constant C are also different for the two GOCART dust emission scheme options. It reads "We note that in addition to the size distribution, the values of empirical proportionality constant C are also different for the two GOCART dust emission scheme options. For dust_opt=13, C value is set to 1.0 $\times 10^{-9}$ kg s^2 m^{-5}, which is consistent with the original GOCART dust emission scheme paper (Ginoux et al., 2001). For dust_opt=1, C value is set to 0.8 $\times 10^{-9}$ kg s^2 m^{-5}." (P7 L155-159).

12. P6 L142: ". . . we cut the size bins for MOSAIC aerosol scheme from Shao2011 directly." Please be clearer on how the emitted dust size bins were configured for both

the GOCART and Shao2011 simulations. The UoC emitted dust size bins have diameter ranges of < 2.5, 2.5–5, 5–10, 10–20 µm in v3.7.1 and 0.2–2, 2–3.6, 3.6–6, 6–12, 12–20 µm in v3.9. UoC emitted dust size bins from v3.9 match the emitted dust size bins from GOCART dust_opt=1. Emitted dust size bins in GOCART dust_opt=13 appear to be modified to ignore dust particles larger than 10 µm and match the 4-bin distribution used by MOSAIC (MOSAIC bins also noted by authors on P5 L109). Does this statement imply the authors modified the MOSAIC module aerosol size bins to incorporate 5 bins and larger particles (particles up to 20 µm) for the simulations configured with Shao2011? Also, the use of the word "cut" here is a little colloquial.

For GOCART dust emission scheme under MOSAIC framework, it first calculates the total dust emission fluxes (P6 Eq. (1)) and then the total dust emissions from 0.2 to 20 µm are redistributed to the size bins of MOSAIC (0.039-0.156, 0.156-0.625, 0.625-2.5 and 2.5-10.0 µm) with mass fractions of 0%, 0.38%, 8.8%, 68.0%. Please also see our reply to specific comment #11 from reviewer #2.
Shao2011 first calculates the emitted dust from 0.98 um to 20 um with 40 size bins. In MOSAIC, dust emissions from these 40 size bins are directly grouped into the four size bins of the MOSAIC aerosol scheme (0.039-0.156, 0.156-0.625, 0.625-2.5, 2.5-10 um). The step that group the size bins to < 2.5, 2.5–5, 5–10, 10–20 µm in v3.7.1 (or 0.2–2, 2–3.6, 3.6–6, 6–12, 12–20 µm in v3.9) is skipped.
We did not modify the MOSAIC module aerosol size bins to incorporate 5 bins and larger particles. For the Shao2011 dust emissions scheme within MOSAIC module, the size bins are also the same as the original MOSIAC size bins (0.039-0.156, 0.156-0.625, 0.625-2.5, 2.5-10 um).
We revised our manuscript accordingly to make the size bins for GOCART (P7 L152-155) and Shao2011 (P7 L169-171) clearer.

13. P7-10 Section 2.3: Please introduce what is meant by important terms like "rebound effect," "collection efficiency from interception," "Schmidt number," and "Stokes number" to help readers understand why differences in these parameters matter for the deposition process.

We added the description for rebound effect in Setc. 2.3 and it reads “When large particles (usually >5 µm) hit the non-sticky surface, they are liable to rebound from the surface if they have sufficient kinetic energy. The rebound factor R represents the fraction of particles that stick to the surface.” (P11 L242-244)

We added the description for collection efficiency from interception in Sect. 2.3.3 and it reads "E_{IN} is the collection efficiency based on the relative dimensions of the particle to the collector diameter (Gallagher, 2002). Interception occurs when particles moving with the mean flow and the distance between an obstacle and particle center is less than half of the diameter. Then the particles will collide with and be collected by the obstacle" (P10 L228-231)
We added the description for collection efficiency from impaction in Sect. 2.3.1 and it reads "E_{IM} is the collection efficiency due to impaction of the particle with the collecting surface (Gallagher, 2002). Impaction occurs when there are changes in the direction of airflow, and particles that cannot follow the flow will collide with the obstacle and stay on the surface due to the inertia (Giardina and Buffa, 2018)." (P9 L194-196)
We added the description for Stokes number in Sect. 2.3.1 and it reads "St is the ratio of the particle stop distance to the characteristic length of the flow and describes the ability of particles to adopt the fluid velocity." (P9 L200-201)

14. P9 L190 and L196: Please provide ranges for the α and A parameters. Does use of Z01 have a dependency on WRF-Chem being configured with a particular land use dataset given the dependency pf γ, α and A on the land use category (LUC)?

Thank you. We added the ranges for the α (P10 L224) and A parameters (P11 L234) in the main text. Yes, USGS land use categories (num_land_cat=24) should be used when using Z01 dry deposition scheme. As the default setting of land use categories is not USGS since WRF v3.8, we added this important information in Sect. 2.4. It reads "We note here that the USGS LUC should be selected for Z01 dry deposition scheme". (P12 L273-274).

15. P10 Section 2.4: Please include the number of vertical levels used and the time step in the model description section.

Thanks. We added the number of the vertical levels in Sect 2.4. It reads "… and 35 vertical levels with model top pressure at 50hPa" (P11 L252-253)
We added the time step in Sect 2.4. It reads "The simulation period is from 26 April to 7 May 2017 with time step of 60s and frequency of output every hour." (P12 L254)

16. P10 L214-215: This section needs a figure showing the model domain or a reference to one of the other figures showing the whole model domain. Suggest expanding Figure 4 (WRF-Chem EROD parameter) to include the whole model domain, changing Figure 4 to Figure 1, and referencing the EROD parameter in the dust emission scheme description section.

Thanks for the suggestion. Now we expanded Fig.4 and changed it to Fig.1. And we referenced the erodibility factor (Fig.1) in the GOCART dust emission scheme description sector (P6 L144). We also cited the domain map in Sect. 2.4 (P11 L253).

17. P10 L219-221: The authors note that meteorological conditions are reinitialized every 24 hours, provide two examples of studies that also used this approach, and comment that this approach has been verified to obtain better meteorological fields. The references provided, however, don't really support this statement. For example, Su and Fung (2015) reinitialize their meteorological fields ever 4 days, and neither study explored the use of different "spin-up" approaches on their results. Reinitialization or "daisy-chain" spin-up is a common practice used by numerical weather modelers. As long as the resultant weather fields used in the experiment were representative, the justification statement (L220-221) is unnecessary.

We now evaluated the meteorological conditions (see Fig. 2 and Table 4 and the discussion in the beginning of the result section) (Sect. 3. 1 P14 L303-324). The weather fields are very similar in all experiments and close to the reanalysis dataset we used to drive the model. So we removed the justification statement in Sect. 2.4. (P12 L264-265)

18. P11 Section 3 (Results): MOSAIC incorporates aerosol feedbacks. The six tests most likely were subject to different weather forcing conditions as the simulations evolved. How notable were those differences?

We evaluated the meteorological conditions in six different experiments and found the difference is very small. Take the weather conditions at 06:00 UTC on 3 May (Figure S2) as an example, we can see that the wind field at 10 meters and temperature at 2 meters are almost the same among six experiments. We also calculated the correlation coefficient and RMSE of wind field at 10 meters and temperature at 2 meters between simulated weather conditions and FNL data (Table

S2). The correlation coefficients for all the experiments are almost the same (Table S2). Although aerosol feedback is turned on, the effect on weather conditions is small, probably because we reinitialized the meteorological condition every 24 hours.
We described the weather forcing difference of the six experiments in Sect. 3.1(P14 L322 P15 L323-324).

19. P11 L241-242: The authors utilize AOD simulation results at 1300 local time to compare with the daily MODIS AOD product. The actual model domain encompasses multiple time zones though (e.g., Fig. 1). Are the model values used for the analysis based on the central point of the model domain (UTC + 8 hours), or was there some other approach used to create a composite simulation product? A comparison of a single simulation time period to the daily product may be fine if the model correctly captured the timing of the forcing conditions. Was this the case? If not, it may be better to compare the daily MODIS product to the simulation time period that best matches the state of the atmosphere when the observations were collected or use simulated daily averaged-AOD values for the comparison.

The model values used for the analysis are not based on the central point of the model domain. We extracted the model results at 13:00 local time for each region. First, we divided the domain into different time zones according to the longitude. Then we can get the UTC when the local time is 13:00 in different time zones. Next, the simulated AOD results are extracted at the corresponding UTC to build an AOD map for the entire domain for each day. Finally, these processed daily model results are compared with the MODIS daily AOD data. For example, for the UTC+8 Time Zone with longitude near 120E, we use the WRF-Chem simulated AOD at 05:00 UTC to compare with the MODIS daily AOD data. And for the UTC+6 Time Zone with longitude near 90E, we use the WRF-Chem simulated AOD at 07:00 UTC to compare with the MODIS daily AOD data.
As the A-Train satellites pass most region of Earth at around 13:30 local time, we think it is more reasonable to use the model results at 13:00 local time in each region to compare with MODIS daily AOD data.
We also revised our description of the comparison method to make it clear in Sect. 2.5.2. It reads “For the model results, first we divided the domain into different time zones according to the longitude. Then the model results at corresponding UTC when the local time is 13:00 are extracted. The collocated model AOD results for each day are used to compared with daily MODIS AOD.” (P13 L289-292)

20. P11-12 L245-256: Which dry deposition scheme was used for the dust emission analysis? MOSAIC includes aerosol feedbacks, which could affect the surface winds driving the dust emission simulation. The authors state that they reinitialized the meteorological conditions every 24 hours, but that could still allow enough time for the forcing conditions to be affected. Were the wind fields the same in both emission scheme tests?

In the revised manuscript, Z01 dry deposition scheme is used for all the dust emission analysis. In our original manuscript, the BS95 dry deposition scheme was used for the Sect. 3.2, the Z01 dry deposition was used for the Appendix B. We now also use the Z01 for dust emission analysis in Sect. 3.2 for consistency in the revised manuscript. When using one dust emission scheme, the dust emission difference between different dry deposition schemes is very small even though dust concentrations are significantly different using different dry deposition schemes. Dry deposition schemes affect dust emission process by influencing forcing conditions through aerosol feedbacks. But this influence is very small in our study, as simulated meteorological fields are very similar among different experiments. Please also see our reply to specific comment #18 from reviewer #2.

21. P12 L258: Why was this time period chosen? Is it the highest magnitude of dust emission for the simulation event?

Yes. This time period is almost the highest magnitude of dust emission for the simulation event. We use this time period as an example to discuss about the reasons for the dust emission flux difference from different dust emission schemes, and we can expect the same results in other time period.

22. P12 L263-264 and L268-269: Unless the authors have altered the code, Shao2011 as implemented in WRF-Chem uses the EROD parameter from the original GOCART dust emission scheme as a mask. Dust emission is permitted where the erodibility factor is greater than zero via a binary (0 or 1) multiplier (e.g., LeGrand et al., 2019; section 3.3; implemented in module_uoc_dust.F). Note, areas classified as zero in the default pre-calculated erodibility factor dataset in WRF-Chem over land are either relatively high points in the terrain (maximum elevation in the surrounding 10◦×10◦ area) or determined to have vegetation coverage according to a static 1987 annual average land cover dataset derived from 1◦×1◦ resolution AVHRR data (see Kim et

al., 2013). Was this erodibility factor masking treatment included in the code implemented by the authors into MOSAIC? If not, this is an important distinction to document.

Yes. The erodibility factor masking treatment is included in the code when we implemented Shao2011 into MOSAIC. We added this information in Sect. 2.2.2. It reads "In Shao2011, the erodibility factor is only used to constrain the potential emission regions. Dust emission is permitted in Shao2011 where the erodibility factor is greater than zero." (P8 L167-168)

23. P12 L257-258 and P36 Figure 3: What grain size(s) were used to diagnose u∗t and ut (Fig. 3c through 3f)? Are the dust emission fluxes presented in Fig 3. (g and h) representative of the emission flux for that grain size or the total dust emission flux?

For Shao2011 dust emission scheme, u_{*t} (Fig.5c) is the smallest u*t among all the size bins. For GOCART dust emission scheme, u_t (Fig.5d) is the smallest u_t among all size bins. As u*t and ut decrease with the increasing particle diameter in these two dust emission schemes, u*t and ut are for the largest size bin. Because once the $u_t > u_{*t}\_min$ or $u_{10} > u_t\_min$, there will be dust emissions in this region. The dust emission fluxes presented in Fig.5 is the total dust emission flux (0-10 μm).

24. P12 L269-270: The authors' comment that differences in dust emission flux produced by the two dust emission schemes are due to differences in threshold conditions required for dust emission and differences in formulas and parameters used for calculating dust emission. In other words, the two dust emission schemes are very different from each other and produce different results? This has been well documented in other publications and doesn't add to the discussion. Suggest removing this sentence. The narrative flows into the next paragraph without it.

Yes, the two dust emission schemes have different dust emission mechanisms and are very different from each other. We followed the reviewer's suggestion and removed this sentence (P16 L350-351).

25. P12 L272-275: GOCART is also dependent on mean wind shear. Intermittent turbulence is not considered in the GOCART dust emission process either. Dust emission under low wind speed in GOCART from the Taklimakan Desert is likely due to the threshold velocity error described in LeGrand et al. (2019). The erodibility

factor values in the authors' model domain max out at 0.35. The application of the erodibility factor decreases the dust emission flux.

Thanks! We modified our manuscript accordingly. We added the threshold velocity formulation (Eq. (2) and Eq. (3)) for GOCART dust emission scheme in Sect.2.2.1 (P7 L146-152). Then we added the explanation for the dust emission from GOCART at low wind speed over the TD in Sect. 3.2. It reads "One reason may be the formula used to calculate the threshold velocity (Eq. (3)). The formula used to calculate threshold velocity is from Marticorena and Bergametti (1995), which was originally designed to calculate threshold friction velocity (see (LeGrand et al., 2019) for details). This inconsistency leads to very small threshold velocity in GOCART, which may result in dust emission at low wind speed." (P16 352-356)

26. P13 L280-285: This is an important aspect of the experimental design and needs to be moved to the methodology section/incorporated into Section 2.2. Details about the Shao2011 configuration used in this study should be consolidated to Section 2.2; they should not split between the main text and the appendix.

Thank you for the suggestions. For the first suggestion, we moved this part into Sect. 2.2.2 accordingly (P8 L173-175). For the second suggestion, if we want to make clear the Shao2011 configuration used in this study, we need to describe the details of Shao2011 dust emission scheme and the difference between different WRF-Chem versions of Shao2011 first. But these descriptions will take up lots of space, readers may get stuck and miss the main point (dry deposition part) of our paper. For those readers who are interested in the Shao2011 scheme and the difference between different versions, they can easily go to Appendix A and Appendix B for more details. In this way, we can ensure the fluency of our paper without losing specific details.

27. P13 L294-295: Please provide a reference for the statement "As desert dust mass is mainly concentrated in the large particle size range. . ." and the upper bound of the range. Is this statement appropriate for all desert regions or just East Asia? Also please include the value of the reference diameter (5 μm) in the main text as well as the figure caption. The "coarse" and "accumulation" characterization of emitted dust from MOSAIC needs to be described prior to this discussion. These are somewhat ambiguous terms in the dust literature. Suggest defining these terms in section 2.2.

Thanks for the suggestion. We added the references for this statement (Kok, 2011; Zhao et al., 2013) (P17 L380). As mentioned in Zhao et al. (2013), the dust size distribution from Kok (2011) (nearly 90% for particle diameter > 2.5 μm) has been evaluated and implemented to North Africa, North America, East Asia and Arabian Peninsula (Chen et al., 2013; Kalenderski et al., 2013; Zhao et al., 2011, 2012).
We included the value of the reference diameter (5 μm) in the main text (P17 L381-382). Now the "coarse" and "accumulation" mode is described in Sect 2.1 (P5 L118-119).

28. P15 L350: Suggest replacing the phrase "better than" with "more physically meaningful" here (also in the abstract). "Better physics" does not always translate to better numerical model simulations.

Thanks! This is now incorporated in the main text (P19 L436-437). In the abstract, we used the phrase "a better physical treatment" which is similar to the phase "more physically meaningful".

29. P16 L373: "Extremely high AOD" is a little too vague here. Are the observed AOD values considered extremely high for this type of event in East Asia? Suggest replacing the sentence intro with "The highest AOD values for this case study were observed in. . ."

Thanks for the suggestion! The text is now updated (P20 L462-463).

30. P17 L376-377: Wording here is a little odd. Suggest changing to "Simulated AOD values from the S11Z01 configuration produced the closest match to the observed daily MODIS AOD with respect to magnitude and spatial pattern (Fig.8g).

Thanks for the suggestion! The text is now updated (P20 L468 P20 L469-470).

31. P17 L382-383: Was the cloud cover an issue? Were there any areas masked out for clouds in the MODIS AOD observations that may have actually been high in dust concentration?

Thanks for the question. Cloud cover can be potentially an issue for MODIS AOD. In the MODIS C6 Deep Blue aerosol retrieval algorithm, the retrieval is not performed for cloud- or snow/ice-contaminated pixels. Because this dust storm is triggered by a

strong cyclone system, it is accompanied by cloud systems. In the areas masked out by MODIS, there may be dust under the cloud, or it may be uplifted into the cloud. The comparison between simulated AOD and MODIS AOD just performed for the grid points with valid MODIS AOD retrieval. During the simulation period, large areas of our domain contain no valid MODIS AOD retrieval (Fig. 9). So this may lead to the low correlation coefficient in Table 6.

32. P18 L408-409: Reference needed for the statement ". . . dust emitted from [the] Gobi Desert is the most important source of dust weather in northern China."

We added the reference Chen et al. (2017b) for this statement (P22 L514).

33. P18 L409-410: The paper by Su and Fung (2015) provides an analysis of a single case study event in East Asia. This study offers valuable information, but a single case study is not sufficient evidence to make general claims about model performance over a region. Recommend removing the statement about the Shao2011 scheme being documented to give better performance than GOCART over East Asia from the text. It's unnecessary.

Thank you for your suggestion. This sentence has been removed (P22 L516-517).

34. P19 L424: Why is there an ellipsis (. . .) in Eq. A2?

Thanks. We deleted the ellipsis (now is Eq.A3) (P23 L535).

35. P19 L431-432, P30 L446-447, L463-464, P33 Table B1, P35 Table B3: Suggest adding a subscript to β from Eq. A4 since the β symbol is also used to represent a different parameter in one of the deposition schemes.

Thank you for your suggestion. Now we change the β symbol to β_0 in Shao2011 dust emission scheme.

36. P30 Table 3: Columns for dust_opt and dust_schme are unnecessary. The value used to activate the Shao2011 dust emission module by the authors may not be the one used by the WRF-Chem source code managers. Listing an arbitrary setting in Table 3 could cause confusion to readers if this new approach is eventually

implemented into the baseline code with different activation options later. Suggest noting that GOCART is dust_opt=13 and that Shao2011 is dust_opt=4 with dust_schme=3 in the text in section 2.2 and removing these columns from the table.

We agree and removed these columns (P35 Table 3). And we added the corresponding options of dust_opt of GOCART (Sect. 2.2 P6 L129-130) and Shao2011(Sect. 2.2 P6 L132-134).

37. P33 Table B1: The values for the third row seem to be missing.

Thanks. We added the number of types of η_{mi} in the third row of Table B1.

38. P37 Figure 2: The diameter of the emitted dust is less than 10 µm in the dust_opt=13 version of GOCART. Unless the authors have modified the code, the upper range of the emitted dust size bins from dust_opt=3 is 20 µm (in both v3.7.1 and v3.9).

Please see our reply to specific comment #12 from reviewer #2. For the Shao2011 dust emission scheme within MOSAIC module, the upper range of the emitted dust size bins are also 10 µm.

Noted Typos:

1. P14 L302 and P40 Fig 5: Be consistent with symbol case. The particle diameter is represented by a lower case d in all previous equations.

Thanks. The representation of particle diameter has changed to lower case.

2. P11 L241-242: Use of "p.m." is unnecessary with 24-hour clock time.

Corrected.

3. P12 L253: Use of acronym GD for Gobi Desert before it's been defined (on P13 L277).

Corrected. We now first give the definition of the acronym GD (P15 L330) and then use it.

4. P12 L254: Use of acronym TD for Taklimakan Desert before it's been defined (on P12 L271).

Corrected. We now first give the definition of the acronym TD (P15 L329) and then use it.

5. P16 L372: ". . .with MODIS [is provided] in Fig. 8."

Corrected.

6. Punctuation is an issue. Several commas missing from compound sentences throughout the text.

Corrected.

7. Missing the word "the" before desert names throughout the text.

Improved. We corrected this through the text.

References

Chen, S., Huang, J., Zhao, C., Qian, Y., Leung, L. R. and Yang, B.: Modeling the transport and radiative forcing of taklimakan dust over the tibetan plateau: A case study in the summer of 2006, J. Geophys. Res. Atmos., 118(2), 797–812, doi:10.1002/jgrd.50122, 2013.

Chen, S., Huang, J., Qian, Y., Zhao, C., Kang, L., Yang, B. and Wang, Y.: An Overview of Mineral Dust Modeling over East Asia, , 31(August), doi:10.1007/s13351-017-6142-2.1.Introduction, 2017a.

Chen, S., Huang, J., Kang, L., Wang, H., Ma, X., He, Y., Yuan, T., Yang, B., Huang, Z. and Zhang, G.: Emission, transport, and radiative effects of mineral dust from the Taklimakan and Gobi deserts: Comparison of measurements and model results, Atmos. Chem. Phys., 17(3), 2401–2421, doi:10.5194/acp-17-2401-2017, 2017b.

Gallagher, M. W.: Measurements and parameterizations of small aerosol deposition velocities to grassland, arable crops, and forest: Influence of surface roughness length on deposition, J. Geophys. Res., 107(D12), 4154, doi:10.1029/2001JD000817, 2002.

Giardina, M. and Buffa, P.: A new approach for modeling dry deposition velocity of particles, Atmos. Environ., 180(September 2017), 11–22,

doi:10.1016/j.atmosenv.2018.02.038, 2018.
Kalenderski, S., Stenchikov, G. and Zhao, C.: Modeling a typical winter-time dust event over the Arabian Peninsula and the Red Sea, Atmos. Chem. Phys., 13(4), 1999–2014, doi:10.5194/acp-13-1999-2013, 2013.
Kang, J. Y., Yoon, S. C., Shao, Y. and Kim, S. W.: Comparison of vertical dust flux by implementing three dust emission schemes in WRF / Chem, , 116(May), 1–18, doi:10.1029/2010JD014649, 2011.
Kok, J. F.: A scaling theory for the size distribution of emitted dust aerosols suggests climate models underestimate the size of the global dust cycle, Proc. Natl. Acad. Sci. U. S. A., 108(3), 1016–1021, doi:10.1073/pnas.1014798108, 2011.
LeGrand, S. L., Polashenski, C., Letcher, T. W., Creighton, G. A., Peckham, S. E. and Cetola, J. D.: The AFWA dust emission scheme for the GOCART aerosol model in WRF-Chem v3.8.1, Geosci. Model Dev., 12(1), 131–166, doi:10.5194/gmd-12-131-2019, 2019.
Marticorena, B. and Bergametti, G.: Modeling the atmospheric dust cycle: 1. Design of a soil-derived dust emission scheme, J. Geophys. Res., 100(D8), 16415, doi:10.1029/95JD00690, 1995.
Su, L. and Fung, J. C. H.: Sensitivities of WRF-Chem to dust emission schemes and land surface properties in simulating dust cycles during springtime over East Asia, J. Geophys. Res. Atmos., 120(21), 11,215-11,230, doi:10.1002/2015JD023446, 2015.
Wu, C.-L. and Lin, Z.-H.: Impact of two different dust emission schemes on the simulation of a severe dust storm in East Asia using the WRF/Chem model, Clim. Environ. Res. (in Chinese), 19(4), 419–436, doi:10.3878/j.issn.1006-9585.2013.13041, 2014.
Yuan, T., Chen, S., Huang, J., Zhang, X., Luo, Y., Ma, X. and Zhang, G.: Sensitivity of simulating a dust storm over Central Asia to different dust schemes using the WRF-Chem model, Atmos. Environ., 207(March), 16–29, doi:10.1016/j.atmosenv.2019.03.014, 2019.
Zhang, X. X., Sharratt, B., Lei, J. Q., Wu, C. L., Zhang, J., Zhao, C., Wang, Z. F., Wu, S. X., Li, S. Y., Liu, L. Y., Huang, S. Y., Guo, Y. H., Mao, R., Li, J., Tang, X. and Hao, J. Q.: Parameterization schemes on dust deposition in northwest China: Model validation and implications for the global dust cycle, Atmos. Environ., 209(April), 1–13, doi:10.1016/j.atmosenv.2019.04.017, 2019.
Zhao, C., Liu, X., Leung, L. R. and Hagos, S.: Radiative impact of mineral dust on monsoon precipitation variability over West Africa, Atmos. Chem. Phys., 11(5), 1879–1893, doi:10.5194/acp-11-1879-2011, 2011.
Zhao, C., Liu, X. and Leung, L. R.: Impact of the Desert dust on the summer monsoon system over Southwestern North America, Atmos. Chem. Phys., 12(8), 3717–3731, doi:10.5194/acp-12-3717-2012, 2012.
Zhao, C., Chen, S., Leung, L. R., Qian, Y., Kok, J. F., Zaveri, R. A. and Huang, J.: Uncertainty in modeling dust mass balance and radiative forcing from size parameterization, Atmos. Chem. Phys., 13(21), 10733–10753, doi:10.5194/acp-13-10733-2013, 2013.

WRF-Chem v3.9 simulations of the East Asian dust storm in May 2017: modeling sensitivities to dust emission and dry deposition schemes

Yi Zeng[1,2], Minghuai Wang[1,2], Chun Zhao[3], Siyu Chen[4], Zhoukun Liu[1,2], Xin Huang[1,2], Yang Gao[5]

[1]Institude for Climate and Global Change Research and School of Atmospheric Sciences, Nanjing University, 210023 Nanjing, China

[2]Joint International Research Laboratory of Atmospheric and Earth System Sciences & Institute for Climate and Global Change Research, Nanjing University, China

[3] School of Earth and Space Sciences, University of Science and Technology of China, Hefei, 230026, China

[4]Key Laboratory for Semi-Arid Climate Change of the Ministry of Education, College of Atmospheric Sciences, Lanzhou University, Lanzhou, 730000, China

[5]Key Laboratory of Marine Environment and Ecology, Ministry of Education/Institute for Advanced Ocean Study, Ocean University of China, and Qingdao National Laboratory for Marine Science and Technology, Qingdao, 266100, China

Correspondence to: Minghuai Wang (minghuai.wang@nju.edu.cn)

Abstract

Dust aerosol plays an important role in the radiative budget and hydrological cycle, but large uncertainties remain for simulating dust emission and dry deposition processes in models. In this study, we investigated dust simulation sensitivity to two dust emission schemes and three dry deposition schemes **for a severe dust storm during May 2017 over East Asia** using Weather Research and Forecasting model coupled with chemistry (WRF-Chem). Results showed that simulated dust loading is very sensitive to different dry deposition schemes, with the relative difference of dust loading using different dry deposition schemes range from 20%-116%. Two dust emission schemes are found to produce significantly different spatial distribution of dust loading. The difference of dry deposition velocity in different dry deposition schemes comes from the parameterization of collection efficiency from impaction and rebound effect. An optimal combination of dry deposition scheme and dust emission scheme has been identified to best simulate the dust storm in comparison with observation ~~and to~~

include better physical treatment of dust emission and surface collection processes. The optimal dry deposition scheme accounts for the rebound effect and the its collection efficiency from impaction changes with the land use categories and therefore has a better physical treatment of dry deposition velocity. Our results highlight the importance of dry deposition schemes for dust simulation.

1 Introduction

Dust aerosol is an important component in the atmosphere and it can impact many processes of the Earth system. Through absorbing and scattering shortwave and longwave radiative fluxes, dust can alter the radiative budgets, which is called the direct effect (Chen et al., 2013; Kok et al., 2017; Zhao et al., 2010, 2011, 2012). Acting as cloud condensation nuclei (CCN) and ice nuclei (IN), dust can change cloud properties and precipitation, which is called the indirect effects (Creamean et al., 2013; Demott et al., 2010). Besides, dust aerosol can absorb solar radiation and change the atmospheric stability and therefore cloud formation, which is known as the semi-direct effect (Hansen et al., 1997). Furthermore, natural dust is important for air quality assessments and has significant impacts on human health (Abuduwaili et al., 2010; Chen et al., 2019; Hofer et al., 2017; Jiménez-Guerrero et al., 2008; Ozer et al., 2007). Although great progress has been made in dust models and dust simulations in recent decades, large uncertainties remain in dust simulations (Huneeus et al., 2011; Prospero et al., 2010; Todd et al., 2008; Uno et al., 2006; Zender et al., 2004; Zhao et al., 2013).

A complete description of dust events includes dust emission, deposition and transport processes. The differences of dust simulation mainly result from the uncertainties of dust emission, deposition and transport processes in models. One uncertainty is from dry deposition processes. Dry deposition refers to the transport of particles from the atmosphere to the Earth's surface in the absence of precipitation (Seinfeld and Pandis, 2006). In most aerosol modeling, dry deposition velocity V_d is used to calculate the dry deposition flux and V_d is usually modelled using the resistance-based approach (Pryor et al., 2008). In the resistance-based approach, V_d is determined by gravitational settling, aerodynamic resistance and surface resistance. Surface resistance is determined by collection efficiency from Brownian diffusion, impaction and interception and is corrected for particle rebound. Slinn (1982) proposed a semi-analytical description of particle collection efficiencies based on the wind tunnel studies, and many dry deposition schemes since then are variants of this model (Binkowski and

Shankar, 1995; Giorgi, 1986; Peters and Eiden, 1992; Zhang et al., 2001). As the formulations for collection efficiencies from different dry deposition schemes are derived from measurements that have been obtained under different meteorological conditions and land surface types, there remains a large discrepancy of these formulations between different dry deposition models (Petroff et al., 2008).

At present, the comparisons of different dry deposition schemes with reliable field measurements are mainly focused on one-dimensional dry deposition models (Hicks et al., 2016; Khan and Perlinger, 2017; Petroff et al., 2008; Ruijrok et al., 1995). For example, Hicks et al. (2016) compared five deposition models with observations and found that V_d predicted for particles less than 0.2 μm is consistent with the measurements, but predicted V_d can vary greatly in the size range of 0.3 to about 5 μm. However, few studies have been conducted to study how different dry deposition schemes affect aerosol concentrations and their spatial distribution in the 3D numerical models. Wu et al. (2018) compared the effects of different dry deposition schemes on black carbon simulation in a global climate model (CESM-CAM5), but did not examine how different dry deposition schemes affect aerosol concentrations for large-size aerosol particles **(e.g., diameters > 2.5 μm)**, such as dust.

Another uncertainty of dust simulation is the treatment of dust emission process in models. Natural dust is typically emitted from dry, erodible surfaces when the wind speed is high. Dust emission process is closely related to soil texture, soil moisture content, surface conditions, atmospheric stability and the wind velocity (Marticorena and Bergametti, 1995). Dust emission schemes are used to predict the dust emission flux and to describe the dust size distribution. Many studies have compared and evaluated the performance of different dust emission schemes (Kang et al., 2011; LeGrand et al., 2019; Su and Fung, 2015; Wu and Lin, 2013, 2014; Yuan et al., 2019; Zhao et al., 2010, 2006). These studies show large diversity of simulated dust emission flux among different dust emission schemes. Zhao et al. (2006) implemented two dust emission schemes in the NARCM (Northern Aerosol Regional Climate Model) regional model, and found that both schemes captured the dust mobilization episodes and produced the similar spatial distributions of dust loading over East Asia, but **significant differences exist in** the dust emission fluxes and surface concentrations ~~differ a lot~~. Kang et al. (2011) compared three dust emission schemes in WRF-Chem and found that the difference between the vertical dust fluxes derived from the three emission schemes can reach to several orders of magnitude. Yuan et al. (2019) found that one scheme strongly

underestimated the dust emission while another two schemes can better show the spatial and temporal variation of dust AOD based on **WRF-Chem simulation of** a storm outbreak in Central Asia. **In another WRF-Chem study,** ~~These differences mainly come from the dust emission flux parameterizations and differences in soil and surface input parameters in different dust emission schemes (~~Chen et al.~~,~~ **(**2017) **concluded that the dust emission differences mainly come from the dust emission flux parameterizations and differences in soil and surface input parameters in different dust emission schemes.**

While dust emission schemes have been studied quite extensively, few studies have examined dust emission and dry deposition schemes simultaneously. As both dust emission schemes and dry deposition schemes contribute significantly to the uncertainties in dust simulations, evaluating dust schemes based on a single dry deposition scheme may be problematic, especially if the dry deposition schemes employed have deficiency. For example, as a widely used regional model that has been coupled with a variety of dust emission schemes, the WRF-Chem model has been used in many studies to evaluate the performance of dust emission schemes (LeGrand et al., 2019; Su and Fung, 2015; Wu and Lin, 2013, 2014; Yuan et al., 2019). But most of these studies use the GOCART aerosol scheme and only one dry deposition scheme (Wesely et al., 1985) is coupled within the GOCART aerosol scheme. Zhang et al. (2019) compared the modelled dust deposition using the GOCART aerosol scheme in WRF-Chem with observed dust deposition, and found that modelled dust deposition is highly underestimated by more than one order of magnitude compared to the observed deposition. This indicates that the dry deposition scheme (Wesely et al., 1985) in GOCART aerosol scheme may not be suitable for dust simulation and needs to be further improved.

In this study, we adopted the MOSAIC aerosol scheme coupled within the WRF-Chem model to study how dry deposition schemes and dust emission schemes affect dust simulations by evaluating model results against observations. As the MOSAIC aerosol scheme includes several different dry deposition schemes, this allows us to choose more advanced dry deposition schemes. As the default MOSAIC aerosol scheme only includes the GOCART dust emission scheme, we further implemented the dust emission scheme Shao2011 (Shao et al., 2011) in the MOSAIC aerosol scheme, which allows us to compare these two widely used dust schemes along with multiple dry deposition schemes. The goals of this study are: (1) to study dust simulation sensitivity to different dust emission schemes and dry deposition schemes, (2) to explore which

combination of dust emission scheme and dry deposition scheme can better simulate dust storms in East Asia. The paper is organized as follows. Sect. 2 introduces the WRF-Chem model, dust emission schemes and dry deposition schemes used, experiments design and measurements. Sect. 3 analyzes the dust simulation sensitivity to dust emission schemes and dry deposition schemes and the comparisons with observations. Sect. 4 is the summary and discussion.

2 Methodology and measurements

2.1 Model description

In this study, WRF-Chem version 3.9 is used. WRF-Chem is built based on the regional mesoscale model WRF, and fully coupled with gas and aerosol chemistry module (Grell et al., 2005). **A summary of the settings used to configure the model is listed** ~~The model setups are listed~~ in Table 1. The Noah land surface model (Chen and Dudhia, 2001) and the Yonsei University (YSU) planetary boundary scheme (Hong et al., 2006) are used in this study. **The global soil categorization data set from the United States Geological Survey (USGS) with 24 land categories are used.** The Rapid Radiative Transfer Model for General Circulation (RRTMG) radiation scheme (Iacono et al., 2008) is used to calculate the longwave and shortwave radiation. The Grell-Freitas convective scheme (Grell and Freitas, 2014) and the Morrison two-moment microphysics scheme (Morrison et al., 2008) are used. The gas-phase chemistry module used is the Carbon-Bond Mechanism version Z (CBMZ, Zaveri and Peters, 1999). The aerosol module used here is the Model for Simulating Aerosol Interactions and Chemistry with 4 bins (MOSAIC 4-bin) (Zaveri et al., 2008). **The MOSAIC 4-bin aerosol scheme divides airborne particles into four size bins by their effective diameter (0.039-0.156, 0.156-0.625, 0.625-2.5, 2.5-10.0 μm) to represent aerosol size distribution.** ~~The MOSAIC aerosol scheme uses sectional approach to represent aerosol size distribution. The MOSAIC 4-bin aerosol scheme divides aerosol particles into four size bins by aerosol diameter: 0.039-0.156, 0.156-0.625, 0.625-2.5, 2.5-10.0 μm.~~ **The first three bins represent the Aitken mode and accumulation mode of aerosol. The last bin represents the coarse mode of aerosol.** The MOSAIC aerosol scheme includes sulfate, methane sulfonate, nitrate, chloride, carbonate, ammonium, sodium, calcium, black carbon (BC), primary organic mass (OC), liquid water and other inorganic mass (OIN). The OIN species include silica, other inert minerals and trace metals. The emitted dust ~~from dust emission~~

~~schemes~~ is assigned to the OIN class of MOSAIC to simulate the major aerosol processes. To study the sensitivity of dust simulation to different dust emission schemes and dry deposition schemes, we test two different dust emission schemes (see Sect. 2.2) and three dry deposition schemes (see Sect. 2.3) within MOSAIC.

2.2 Dust emission schemes

Dust emission schemes include empirical schemes and schemes based on dust physical processes. Because of differences in input parameters and formulas to calculate dust flux, dust emission varies among different dust emission schemes. The Goddard Chemistry Aerosol Radiation and Transport (GOCART) dust emission scheme (Ginoux et al., 2001) is an empirical scheme and was implemented in MOSAIC by Zhao et al. (2010). **The GOCART dust emission scheme within MOSIAC aerosol scheme is called by setting dust_opt=13.** The University of Cologne (UoC) dust emission schemes (Shao, 2001, 2004; Shao et al., 2011) (Shao schemes) are size-resolved dust emission scheme based on the wind erosion physical theory. **The UoC dust emission scheme within GOCART aerosol scheme is called by setting dust_opt=4. When the UoC dust emission scheme is selected, the user should also choose one of the UoC sub-options by setting dust_scheme=1 for Shao2001, dust_schme=2 for Shao2004, or dust_schme=3 for Shao2011.** ~~Shao2011 (Shao et al., 2011) is a simplified version of Shao2004 (Shao, 2004), but the performances of the full scheme (Shao2004) and the simplified scheme are equally effective (Shao et al., 2011).~~ The Shao dust emission schemes are widely used for dust simulations in East Asia, and have been found to perform well in simulating dust emission fluxes (Shao et al., 2011; Su and Fung, 2015; Wu and Lin, 2014)**, and Shao2011** (Shao et al., 2011) **is a simplified version of Shao2004** (Shao, 2004). To test the sensitivity of dust simulation to different dust emission schemes, we implemented the Shao2011 dust emission scheme in MOSAIC **aerosol scheme**. Each dust emission scheme is described in detail below.

2.2.1 GOCART

The formula of vertical dust flux in GOCART is approximated as:

$$F_p = \begin{cases} CSs_p u_{10}^2 (u_{10} - u_t) & \text{if } u_{10} > u_t \\ 0 & \text{otherwise} \end{cases} \quad (1)$$

where C is an empirical proportionality constant, and S is the source function **that is determined by the erodibility factor**

(see Fig.1). s_p is the fraction of each size class of the emitted dust. u_{10} is the horizontal wind speed at 10 meters. u_t is the threshold velocity below which the dust emission does not occur. u_t **is calculated as:**

$$u_t = u_{t0} * (1 + 1.2\, log_{10}\, w) \quad (2)$$

where u_{t0} **is the threshold velocity for dry soil and w is the soil surface wetness. The formula of** u_{t0} **is not from the original GOCART paper** (Ginoux et al., 2001)**, but from** ~~(~~Marticorena and Bergametti~~,~~ (1995) **:**

$$u_{t0} = 0.129 \frac{\left(\frac{\rho_p g d_p}{\rho_a}\right)^{0.5}\left(1+\frac{0.006}{\rho_p g d_p^{2.5}}\right)^{0.5}}{\left[1.928\left(a(d_p)^x+b\right)^{0.092}-1\right]^{0.5}} \quad (3)$$

where ρ_p **is the density of particles,** ρ_a **is the density of air,** d_p **is particle diameter, a equals 1331, x equals 1.56 and b equals 0.38. The original GOCART dust emission scheme in GOCART aerosol scheme (dust_opt=1) calculates the dust emission flux from 0.2 to 20 μm. For GOCART dust scheme in MOSAIC aerosol scheme (dust_opt=13), the total dust emissions from 0.2 to 20 μm are redistributed to the size bins of MOSAIC (0.039-0.156, 0.156-0.625, 0.625-2.5 and 2.5-10.0 μm) with mass fractions of 0%, 0.38%, 8.8%, 68.0%** (Kok, 2011; Zhao et al., 2013)**. We note that in addition to the size distribution, the values of empirical proportionality constant C are also different for the two GOCART dust emission scheme options. For dust_opt=13, C value is set to 1.0 ×10^{-9} kg s^2 m^{-5}, which is consistent with the original GOCART dust emission scheme paper** (Ginoux et al., 2001)**. For dust_opt=1, C value is set to 0.8 ×10^{-9} kg s^2 m^{-5}.** ~~The emitted dust emission flux from GOCART scheme is re-distributed into different bins for MOSAIC as Zhao et al. (2010).~~

2.2.2 Shao2011

The Shao2011 dust emission scheme is a size-resolved dust emission scheme based on the wind erosion physical theory. The dust flux is determined by:

$$F(d_i) = c_y \eta_{mi}(1+\sigma_m)\frac{gQ}{u_*^2} \quad (4)$$

where $F(d_i)$ is the dust emission rate of particle size d_i; c_y is the dimensionless coefficient; η_{mi} is the mass fraction of free dust for a unit soil mass; σ_m is bombardment efficiency; Q is the saltation flux averaged over the range of sand particle sizes.

In Shao2011, the erodibility factor is only used to constrain the potential emission regions. Dust emission is permitted in Shao2011 where the erodibility factor is greater than zero. As the Shao2011 scheme is a size-resolved dust emission scheme, **it first calculates the emitted dust from 0.98 um to 20 um with 40 size bins. Dust emissions from these 40 size bins are then grouped into the four size bins of the MOSACI aerosol scheme (0.039-0.156, 0.156-0.625, 0.625-2.5, 2.5-10 um)** ~~we cut the size bins for MOSAIC aerosol scheme from Shao2011 directly~~. The details of the Shao2011 dust emission scheme are described in Appendix A. There is a bug in calculating dust emission flux in Shao2011 scheme reported after WRF-Chem v3.9, **and** we have already corrected it in our simulation (See Appendix A). We should mention that the Shao2011 dust emission scheme used in this study **is based on WRF-Chem v3.9 with some modifications from WRF-Chem v3.7.1. The difference of Shao2011 among different WRF-Chem versions are documented in Appendix B.** ~~is not the original version in WRF-Chem v3.9 and the details will be discussed in Sect. 3.1 and Appendix B.~~

2.3 Dry deposition schemes

For dry deposition schemes, dry deposition velocity (V_d) is used to calculate dry deposition flux. V_d is determined by gravitational settling velocity (V_g), aerodynamic resistance (R_a) and surface resistance (R_S). There are three dry deposition schemes available in WRF-Chem coupled with the MOSAIC module and used in this study as referred to BS95 (Binkowski and Shankar, 1995), PE92 (Peters and Eiden, 1992) and Z01 (Zhang et al., 2001). Each dry deposition scheme will be described in detail below.

2.3.1 BS95

In the BS95 scheme (Binkowski and Shankar, 1995), V_d is expressed as:

$$V_d = V_g + \frac{1}{R_a + R_s + R_a R_S V_g} \quad (5)$$

where R_a and R_s are aerodynamic and surface resistance; V_g is the gravitational settling velocity and is given as:

$$V_g = \frac{\rho_p d_p^2 g C_c}{18\mu} \quad (6)$$

where C_c is the Cunningham correction factor as a function of d_p and mean free path of air (λ), and μ is the viscosity

dynamic of air. The surface resistance is calculated as:

$$R_s = \frac{1}{u_*(E_B+E_{IM})} \quad (7)$$

where E_B is collection efficiency from Brownian diffusion. E_B is calculated as follows:

$$E_B = Sc^{-\frac{2}{3}} \quad (8)$$

where Sc is the Schmidt number, given by $Sc = \nu/D$. ν is the kinematic viscosity of air and D is the particle Brownian diffusivity. E_{IM} **is the collection efficiency due to impaction of the particle with the collecting surface (Gallagher, 2002). Impaction occurs when there are changes in the direction of airflow, and particles that cannot follow the flow will collide with the obstacle and stay on the surface due to the inertia (Giardina and Buffa, 2018).** E_{IM} is given by:

$$E_{IM} = 10^{-\frac{3}{St}} \quad (9)$$

where St is the Stokes number, given by:

$$St = \frac{u_*^2 v_g}{gv} \quad (10)$$

St is the ratio of the particle stop distance to the characteristic length of the flow and describes the ability of particles to adopt the fluid velocity (Pryor et al., 2008; Seinfeld and Pandis, 2006)**.**

2.3.2 PE92

In PE92 scheme (Peters and Eiden, 1992), the dry deposition velocity (V_d) is expressed as:

$$V_d = V_g + \frac{1}{R_a+R_S} \quad (11)$$

The formula of V_g and R_a is the same as in BS95, but the way to calculate R_S is quite different. In PE 92, R_S is parametrized as:

$$R_S = \frac{1}{u_*(E_B+E_{IM}+E_{IN})R} \quad (12)$$

where E_{IN} is collection efficiency from interception and R is the factor for particle rebound. E_{IM}, E_{IN} and R are expressed as:

$$E_{IM} = \left(\frac{St}{0.8+St}\right)^2 \quad (13)$$

$$E_{IN} = \frac{(0.0016+0.0061z_0)d_p}{1.414\times10^{-7}} \quad (14)$$

$$R = e^{-2\sqrt{St}} \quad (15)$$

z_0 is the roughness length and d_p is particle diameter. Stokes number is given by:

$$St = \frac{\rho_p d_p^2}{9\mu d_c} u \quad (16)$$

u is the horizontal wind velocity, d_c is the diameter of the obstacle.

2.3.3 Z01

In Z01 scheme (Zhang et al., 2001), the formula of V_d is the same as in BS95 scheme (Eq. (5)). Surface resistance R_S is calculated as:

$$R_S = \frac{1}{\epsilon_0 u_* (E_B+E_{IM}+E_{IN})R} \quad (17)$$

$$E_B = Sc^{-\gamma} \quad (18)$$

where γ depends on land use categories (LUC) and lies between 0.50 and 0.58.

E_{IM} is expressed as:

$$E_{IM} = \left(\frac{St}{\alpha+St}\right)^{\beta} \quad (19)$$

where β equals to 2. α depends on LUC **and lies between 0.6 and 100.0**. The Stokes number is given by:

$$St = V_g u_*/gA \quad (20)$$

over vegetated surfaces (Slinn, 1982) and

$$St = V_g u_*^2/g\nu \quad (21)$$

over smooth surfaces or surfaces with bluff roughness elements (Giorgi, 1988). E_{IN} **is the collection efficiency based on the relative dimensions of the particle to the collector diameter (Gallagher, 2002). Interception occurs when particles moving with the mean flow and the distance between an obstacle and particle center is less than half of the diameter.**

Then the particles will collide with and be collected by the obstacle. E_{IN} is expressed as:

$$E_{IN} = \frac{1}{2}\left(\frac{d_p}{A}\right)^2 \quad (22)$$

over vegetated surfaces and $E_{IN} = 0$ for non-vegetated surfaces, where A is the characteristic radius of collectors. A depends on LUC **and lies between 2.0 mm and 10.0 mm**. R is expressed as:

$$R = e^{-1.0\sqrt{St}} \quad (23)$$

The main difference of formulas used to calculate dry deposition velocity for three different dry deposition schemes are listed in Table 2. For R_S, PE92 and Z01 include the collection efficiency from interception (E_{IN}) and the rebound effect (R), while these two are neglected in BS95. For the E_{IM} parameterization, all three schemes use St to parameterize E_{IM}, but the formulas are quite different. BS95 has a different formula from PE92 and Z01, while the PE92 and Z01 have the same formula but with different coefficients. For PE92, the coefficient for E_{IM} is constant for all the surface types. For Z01, the coefficients α and β for E_{IM} change with different surface types. For the E_{IN} parameterization, BS95 ignores this effect; PE92 and Z01 use different formulas and variables to calculate E_{IN}. **When large particles (usually >5 μm) hit the non-sticky surface, they are liable to rebound from the surface if they have sufficient kinetic energy. The rebound factor R represents the fraction of particles that stick to the surface (Seinfeld and Pandis, 2006).** For rebound effect, BS95 does not consider~~ it~~**it**~~the rebound effect~~; PE92 and Z01 use the same e-exponential form $e^{-b\sqrt{St}}$ to calculate the rebound effect with different coefficient b. For PE92, b is 2.0; for Z01, b is 1.0. In addition, the parameterization of St is quite different for different dry deposition schemes. For BS95, the formulation of St tends to emphasize the nature of the flow field (Binkowski and Shankar, 1995; Pryor et al., 2008). For Z01, the formulation of St is from Slinn (1982) over vegetated surfaces and from Binkowski and Shankar (1995) over smooth surfaces. The formulation of St from Slinn (1982) and Peters and Eiden (1992) are focus on the individual obstacles (Pryor et al., 2008).

2.4 Experiments Design

We use WRF-Chem v3.9 with 20 km × 20 km horizontal resolution **and 35 vertical levels with model top pressure at 50hPa**~~to simulate the dust storm in May 2017~~. The domain covers most of the East Asia (14-60°N, 74-130°E) **as shown in**

Fig. 1. The simulation period is from 26 April to 7 May 2017 **with time step of 60s and frequency of output every hour**. **The timestep between radiation physics calls is 20 minutes.** During this period, a severe dust storm event originated from northwestern China and Outer Mongolia, and air quality deteriorated dramatically in a very short time in downwind areas (Guo et al., 2019; Zhang et al., 2018). Meteorological conditions are initialized and forced at the lateral boundaries using the 6-hourly National Center for Environmental Prediction Final (NCEP/FNL) Operational Global Analysis data at a resolution of 1°×1°. **For meteorological conditions (such as wind speed and temperature), we reinitialized every 24 hours using NCEP/FNL reanalysis data. For chemistry, the output of the aerosol field (such as the concentration of different aerosol species) from the previous 1-day run was used as the initial chemical conditions for the next 1-day run. Our simulation period is from 26 April to 7 May 2017 and one experiment consists of 12 one-day runs. In this way, the chemical field are continuous and we can also get more reliable meteorological conditions.** ~~The meteorological conditions are reinitialized every 24 hours. This method has already been used in other simulations (Su and Fung, 2015; Zhang et al., 2016), which has been verified that a better meteorological field can be obtained. The output of the aerosol field from the previous 1-day run was used as the initial chemical conditions for the next 1-day run.~~ The MOSAIC aerosol scheme was used for all the simulations. Simulation results prior to 28 April are treated as model spin up for chemical initial condition and are not included in results presented in Sect. 3. The model results from 1 May to 7 May are used for the dust loading and concentration analysis. And the model results from 28 April to 7 May are used for the dust emission analysis as the dust emission before 1 May also have influence on the dust concentration during 1 May to 7 May. To study the dust simulation sensitivity to dust emission and dry deposition schemes, we run 6 experiments with two different dust emission schemes and three dry deposition schemes (See Table 3). The corresponding model configuration for ~~dust emission and~~ dry deposition processes of the six experiments also listed in Table 3. **We note here that the USGS LUC should be selected for Z01 dry deposition scheme.**

2.5 Measurements

~~2.4.1~~2.5.1 PM10

Hourly surface observed PM10 is used to compare with the simulated PM10 from WRF-Chem. In China, hourly surface PM10 concentrations were collected from more than 1000 environmental monitoring stations **(locations shown in results section)** maintained by the Ministry of Environmental Protection (MEP). The hourly PM10 data from 1 May to 7 May, 2017 were downloaded from http://beijingair.sinaapp.com/. We collocated the PM10 data to WRF-Chem simulation grids to evaluate model performance with different configurations.

~~2.4.2~~2.5.2 MODIS AOD

Daily aerosol optical depth (AOD) from Moderate Resolution Imaging Spectroradiometer (MODIS) is used to compare with our simulated AOD from WRF-Chem. The MODIS onboard Aqua satellite was launched by the NASA in 2002 and Aqua is a part of A-Train satellite constellation. To compare modelled AOD with observations, we use AOD retrievals at 550 nm from MODIS AOD products on Aqua with daily gridded data at a resolution of 1°×1° (MYD08_D3, Collection 6, combined dark target and deep blue AOD). The MODIS Aqua collection daily MYD08_D3 files were obtained from https://ladsweb.nascom.nasa.gov. As Aqua passes through every region of Earth at **around** 13:30 ~~p.m.~~ local time, we extract the model simulation results at 13:00 ~~p.m.~~ to compare with the daily MODIS AOD. **For the model results, first we divided the domain into different time zones according to the longitude. Then the model results at corresponding UTC when the local time is 13:00 are extracted. The collocated model AOD results for each day are used to compared with daily MODIS AOD.**

2.5.3 CALIPSO data

The vertical profile of aerosol extinction coefficient at wavelength of 532 nm from the Cloud-Aerosol Lidar and Infrared Pathfinder Satellite observation (CALIPSO) satellite is used to evaluate model results. The CALIPSO launched on 28 April 2006 equipped with CALIOP (Cloud-Aerosol Lidar with Orthogonal Polarization). The CALIOP lidar provides an along-track observation of aerosol and cloud vertical profile. The vertical and horizontal resolutions for the CALIOP from the surface to 8.2 km are 30 m and 333 m, respectively. Above 8.2 km, the vertical and horizontal resolutions are 60 m and 1 km, respectively. We use the CALIPSO level 2 APro product (V4.20) to obtain the aerosol

extinction coefficient (CAL_LID_L2_05kmAPro-Standard-V4-20). The CALIPSO data are available at: https://www-calipso.larc.nasa.gov/.

3 Results

3.1 Meteorological conditions

Dust emission and transport processes are closely related to the meteorological conditions. So we first evaluated the model performance in simulating the synoptic conditions. Figure 2 shows the surface meteorological conditions during the dust event. The left panels of Fig.2 show the daily mean wind field at 10 meters and daily mean temperature at 2 meters from NCEP/FNL reanalysis data. The meteorological conditions at 700 hPa show in the supplementary materials (Fig. S1). This dust storm was triggered by the development of a Mongolian cyclone (Fig. S1c and Fig.2c). With the strong southeast and southwest wind near the dust source region, emitted dust was transported to the northeast and southeast of China (Fig. S1c, S1e and Fig. 2c, 2e). Right panels of Fig. 2 show the WRF-Chem simulated daily mean wind field at 10 meters and daily mean temperature field at 2 meters. The meteorological field produced by WRF-Chem are very similar to the NCEP/FNL reanalysis data. In addition, we calculated the correlation coefficient (R) and root mean square error (RMSE) between WRF-Chem simulation and FNL reanalysis data for temperature at 2 meters, U component of wind, V component of wind and wind speed at 10 meters during simulation period (Table 4). The R for time-averaged temperature at 2 meters, U component of wind, V component of wind and wind speed at 10 meters from 1 May to 7 May are 1.0, 0.90, 0.86 and 0.82, respectively. The RMSE for time-averaged temperature at 2 meters, U component of wind, V component of wind and wind speed at 10 meters from 1 May to 7 May are 1.03, 1.08, 0.98 and 1.11, respectively. The R for temperature, U component of wind, V component of wind and wind speed at 700 hPa from 1 May to 7 May are 1.0, 0.94, 0.91 and 0.95, respectively (Table S1). The RMSE for temperature, U component of wind, V component of wind and wind speed at 700 hPa from 1 May to 7 May are 0.67, 2.34, 2.70 and 1.76, respectively (Table S1). Overall, the correlation coefficients are generally large and the RMSEs are generally small. This indicates that the WRF-Chem performed well in simulating the meteorological conditions. We also compared the

difference of the meteorological conditions in our six experiments and found that the difference is negligible (Fig. S2 and Table S2).

~~2.5~~3.2 Dust simulation sensitivity to dust emission schemes

In this section, we examine the changes of the simulated dust loading using different dust emission schemes. Figure 3 shows simulated mean dust loading for six experiments over the 7-day simulation period 1-7 May, 2017. When using the same dry deposition scheme (BS95, PE92 or Z01), different dust emission schemes give very different dust spatial distribution. Compared with the Shao2011 scheme, GOCART has higher dust loading over the Taklimakan desert **(TD)** but has relatively lower dust loading over the Gobi Desert **(GD)**, the south of Outer Mongolia and most parts of northern China. The difference of the spatial distribution of dust loading is mainly caused by the different spatial distribution of dust emission flux from dust emission schemes, as shown in Fig. 4. As the dust emission before 1 May also have influence on the dust loading during 1 May to 7 May, the total dust emission from 28 April to 7 May are analyzed. The total dust emission from 00:00 UTC 28 April to 23:00 UTC 7 May over **the** GD from GOCART and Shao2011 are 4.90 Tg and 13.88 Tg, respectively. The total dust emission from 00:00 UTC 28 April to 23:00 UTC 7 May over **the** TD from GOCART and Shao2011 are 7.16 Tg and 2.75 Tg respectively. Over **the** ~~Gobi Desert~~**GD**, Shao2011 scheme has higher dust emission than GOCART; while over **the TD**~~Taklimakan Desert~~, GOCART scheme has higher dust emission than Shao2011 (Fig. 4c).

The first column of Fig. 5 shows the spatial distribution of friction velocity, threshold friction velocity, the difference between friction velocity and threshold friction velocity and the dust emission flux from Shao2011 at 06:00 UTC on 3 May. The areas where the friction velocity is greater than the threshold friction velocity is mainly located in the west inner Mongolia and the south of Outer Mongolia (Fig. 5e). This is consistent with Fig. 5g. When the friction velocity is larger than threshold friction velocity, dust can be emitted from the surface. The second column of Fig. 5 shows the spatial distribution of wind speed at 10 meters, threshold velocity, the difference between wind speed at 10 meters and threshold velocity and the dust emission flux from the GOCART dust emission scheme. Different from Shao2011, the dust emission regions from GOCART are not only determined by wind speed, but also constrained by erodibility factor (Eq. (1)). From Fig. 5f, the threshold velocity is much smaller than the wind speed at 10 meters in most areas. In these areas, GOCART use Eq. (1) to

calculate the dust emission flux, and the source function S depends on the erodibility factor. The dust emission flux in GOCART is directly scaled by erodibility factor. Figure 1 shows the erodibility factor which describes the fraction of erodible surface in each grid cell. As shown in Fig. 5h, dust emission occurs where the wind speed is high and the erodibility factor is larger than 0. ~~So the difference of dust emission between GOCART and Shao2011 is mainly due to the difference of threshold conditions for dust emission and the difference of formulas and parameters for calculating dust emission flux.~~

Over **the** ~~Taklimakan desert (TD)~~**TD**, Shao2011 produces lower dust emission flux than GOCART. **One reason may be the formula used to calculate the threshold velocity (Eq. (3)). The formula used to calculate threshold velocity is from** ~~(~~Marticorena and Bergametti~~,~~ **(**1995)**, which was originally designed to calculate threshold friction velocity (see** ~~(~~LeGrand et al.~~,~~ **(**2019) **for details). This inconsistency leads to very small threshold velocity in GOCART, which may result in dust emission at low wind speed.** ~~As mentioned by Wu and Lin (2014), there are two possible reasons for this. One is that dust generated by the intermittent turbulence is not considered in Shao2011 scheme. Dust can be generated by the intermittent turbulence rather than by the mean wind shear when the wind speed is low (Klose and Shao, 2012). While GOCART uses the erodibility factor and the empirical formula to calculate the dust emission flux, dust can be emitted where the wind speed is relatively low.~~ Another reason may be the incorrect soil particle size distribution over **the** TD (Wu and Lin, 2014). The incorrect soil particle size distribution can lead to the unreasonable dust emission flux in Shao2011 over **the** TD. Over **the** ~~Gobi Desert (GD)~~**GD**, the GOCART scheme has lower dust emission than the Shao2011 scheme. As mentioned by Su and Fung (2015), the erodibility factor over **the** ~~Gobi Desert~~**GD** is highly underestimated and need to be improved for the GOCART dust emission scheme.

~~We note that~~**As we mentioned in Sect. 2.2.2**, the Shao2011 ~~dust emission scheme we~~ used in this study is based on WRF-Chem v3.9 with some modifications from WRF-Chem v3.7.1 ~~as documented in Appendix B~~. The modified Shao2011 simulates better dust loading than the original Shao2011 scheme in WRF-Chem v3.9 (not shown). Simulated dust emission fluxes ~~can differ a lot~~**are quite different when using** ~~between~~ two versions of the Shao2011 scheme in WRF-Chem v3.9 and WRF-Chem v3.7.1, which is mainly caused by different soil particle size distributions in two versions. The differences of Shao2011 among different WRF-Chem versions are documented in Appendix B.

~~2.6~~3.3 Dust simulation sensitivity to dry deposition schemes

In this section, we analyze dust simulation sensitivity to different dry deposition schemes using the six experiments. For simulated dust loading using the GOCART dust emission scheme (the first row in Fig. 3), compared to the BS95 dry deposition scheme, PE92 and Z01 produce higher dust loading over the dust source regions and remote regions. The relative difference of mean dust loading from PE92 and Z01 relative to BS95 is 20% and 59% respectively. As for the simulated dust loading using the Shao2011 dust emission scheme (the second row in Fig. 3), PE92 and Z01 schemes also produce higher dust loading than BS95 scheme, and the relative difference to BS95 is 72% and 116% respectively. This indicates that dust simulation is very sensitive to dry deposition schemes.

Figure 6a shows the modeled dry deposition velocity over desert surface. As desert dust mass is mainly concentrated in the large particle size range, our dry deposition analysis focuses on the coarse mode **(2.5-10 μm)** (Kok, 2011; Zhao et al., 2013) ~~(near the reference diameter marked as colored dots in Fig. 5)~~. **The reference diameter of the coarse mode is defined at 5 μm (Fig. 6).** BS95 produces larger V_d than PE92 and Z01 in the coarse aerosol mode. Larger V_d leads to larger dry deposition and thus lower dust loading, consistent with the lower simulated dust loading from the BS95 scheme discussed above (Fig. ~~3~~1). In Eq. (5), the dry deposition velocity is comprised of gravitational velocity, aerodynamic resistance and surface resistance. The diversity of different dry deposition schemes mainly comes from the way to parameterize surface resistance, and differences from gravitational settling and aerodynamics resistance are small (not shown), consistent with previous studies (e.g., Bergametti et al., 2018). Figure 6b shows the surface resistance from different schemes as a function of particle diameter **(d_p)**~~(D_p)~~. In the coarse aerosol mode, Z01 produces the largest surface resistance, followed by PE92 and BS95. Larger surface resistance causes smaller dry deposition velocity in Z01, thus larger dust concentration as shown in Fig. ~~3~~1.

The surface collection efficiency is comprised of Brownian diffusion, impaction, and interception and is corrected for particle rebound (see Eq. (12)). Collection from Brownian diffusion is most important for the smaller particles while collection from impaction and interception play a more important role for large particles in surface collection processes. Figure 6c shows the surface collection efficiency from impaction (E_{IM}) from different schemes as a function of particle

diameter. ~~Impaction occurs when there are changes in the direction of airflow, and their inertia carries them across the sublayer to the surface (Seinfeld and Pandis, 2006).~~ BS95 gives the largest E_{IM} and Z01 gives the smallest. Based on field observation data, Slinn (1982) used a semi-empirical fit for smooth surface (Eq. (9)), and Binkowski and Shankar (1995) adopted this formula for E_{IM} and used it for all land surface types. Peters and Eiden (1992) uses Eq. (19) to describe E_{IM}, with α equals to 0.8 and β equals to 2 to get the best fit for the data collected over a spruce forest (Eq. (13)). In Zhang et al. (2001) scheme, α varies with LUC and β is chosen as 2 (Eq. (19)). For BS95 and PE92, the formula of E_{IM} is derived from a specific land surface type, but they have been applied to all land surface types in WRF-Chem. This may lead to large uncertainties for dry deposition over the whole domain with different surface types. As E_{IM} of Z01 varies with LUC, Z01 may have a better physical treatment of E_{IM} than the other two dry deposition schemes.

Figure 6d shows the surface collection efficiency from interception (E_{IN}). ~~Collection from interception occurs when particles moving with the mean flow and the distance between an obstacle and particle center is less than half of the diameter, and~~ E_{IN} depends on the particle diameter and the characteristic radius of the collectors (Seinfeld and Pandis, 2006). E_{IN} is important for large particles on hairs at the leaf surface, and is negligible over non-vegetated surface such as the desert surface we analyzed here (Chamberlain, 1967; Slinn, 1982; Zhang et al., 2001). In BS95, the effect of interception is not considered. In the original PE92 scheme as described in Peters and Eiden (1992), E_{IN} is also not considered. But in the PE92 scheme used in WRF-Chem, E_{IN} increases with particle diameter as in Eq. (14). In Z01, the effect of interception is considered as Eq. (22) over vegetated surface and is not considered for non-vegetated surface (as shown in Fig. 6d over desert surface type). The parameterization of E_{IN} partially results in the difference of surface resistance between PE92 and the other two dry deposition schemes.

Figure 6e shows the rebound factor from different dry deposition schemes. Rebound and resuspension have long been recognized as a mechanism by which the surface can act as sources of particles (Pryor et al., 2008). Due to limited knowledge on particle rebound and resuspension processes, most dry deposition models adopted the form of the rebound effect as $R = e^{-b\sqrt{St}}$ suggested by Slinn (1982) (Zhang and Shao, 2014; Zhang et al., 2001), while some dry deposition schemes do not include the rebound effect with R=1.0 (Binkowski and Shankar, 1995; Petroff and Zhang, 2010; Zhang and He, 2014). BS95 does not consider the rebound effect. b is equal to 2.0 for PE92 scheme and 1.0 for Z01 scheme. Another

difference between PE92 and Z01 is the threshold particle diameter for including the rebound effect. Rebound effect is included for PE92 when particles are larger than 0.625 μm and for Z01 when particles are larger than 2.5 μm. In summary, the smaller E_{IM} and rebound factor lead to larger R_S in Z01, while the larger E_{IM} leads to smaller R_S in BS95, and the moderate E_{IM} and rebound effect give a moderate R_S for PE92.

~~Stokes number is the ratio of the particle stop distance to the characteristic length of the flow, and it describes the ability of particles to adopt the fluid velocity (Pryor et al., 2008; Seinfeld and Pandis, 2006).~~ Figure 6f shows the Stokes number from different dry deposition schemes. Over smooth surfaces, the formula of St for BS95 and Z01 is the same, as shown in Eq. (10). In PE92, St is calculated using Eq. (16), which is similar to the formula used in Slinn (1982). BS95 and Z01 schemes give a larger St than PE92. Stokes number is used to calculate both R and E_{IM}. The difference of Stokes number and the different formulas of R and E_{IM} lead to the different R and E_{IM} among different dry deposition schemes (Fig. 6c and 6e).

Our discussion indicates that Z01 has a better physical treatment of dry deposition velocity, as Z01 considers the rebound effect and E_{IM} changes with LUC. The Z01 scheme has also been documented to agree better with measured dry deposition fluxes and dry deposition velocity (e.g., Zhang et al., 2012; Connan et al., 2018). Zhang et al. (2012) compared the dry deposition fluxes measured at five sites in Taiwan with the modeled dry deposition fluxes and found that the measured dry deposition fluxes can be reproduced reasonably well using the Z01 scheme. Connan et al. (2018) conducted experimental campaigns on-site to determine dry deposition velocity of aerosols and found that the Z01 scheme is most suitable for operational use in the size range 0.2-10 μm. All these indicate that the Z01 dry deposition scheme is ~~better than~~**more physically meaningful than** other two dry deposition schemes.

~~2.7~~3.4 Comparisons with observations

To better evaluate the performance of different experiments, we compared the model results with observations. Figure 7 shows hourly observed PM_{10} concentrations over observational sites at 02:00 UTC on 4 May, 2017 (10:00 Beijing Time (BJT) on 4 May, 2017). Very high PM_{10} values (> 1000 $\mu g\ m^{-3}$) are observed in northern China. Figure 8 compares simulated PM_{10} in six experiments with observed PM_{10}. During the comparison, the observational sites closest to the model grids are paired up. The correlation coefficients (R), root mean square errors (RMSE) between model and observations, and the mean simulated

and observed PM_{10} for all the sites over the five regions during the 7-day period 1-7 May are marked in Fig. 8. The simulated PM_{10} of all the six experiments have obviously underestimated the observations. Among all these experiments, GOBS95 has the lowest average PM_{10} concentration, with a value of 26.45 $\mu g\ m^{-3}$, and S11Z01 has the largest one, with a value of 105.17 $\mu g\ m^{-3}$, the closest one to the observed mean value of 172.70 $\mu g\ m^{-3}$. S11Z01 gives a large R of 0.77 and the smallest RMSE of 96.14 compared to other experiments. Table 5 shows the R and RMSE between the model and observations for PM_{10} for six experiments over five sub regions and over whole China. Over **the** TD, GOBS95 gives the largest R and smallest RMSE. Over **the** GD, GOZ01 and S11Z01 gives a better performance compared with other experiments. For other regions (NCP, NEP and YR), S11Z01 gives a relatively larger R and smallest RMSE. For all the stations in total, S11Z01 gives a larger R of 0.83 and the smallest RMSE of 82.98. Overall, the S11Z01 experiment has the best performance for simulating this dust storm.

Figure **9** shows the MODIS observed daily mean AOD and WRF-Chem simulated AOD **over the simulation period 1-5 May** ~~on 4 May for six experiments~~. For strong dust storms like the one we examined here, dust particles contribute the most to AOD, and AOD therefore can represent the dust loading in the atmosphere. To match the MODIS AOD observation time, simulated AOD at 13:00 ~~p.m.~~ local time is used for comparison **(see Sect. 2.5 for details)**. For each 1 °×1° grid with observed AOD from MODIS, the average value of simulated AOD from WRF-Chem in this grid is calculated. **Grid points without valid MODIS AOD retrieval are masked for both observational and model results in Fig. 9. A major dust emission event occurred over the GD on 3 May (Fig. 9c). Shao2011 well simulated the dust emission event over the GD on 3 May (Fig. 9m), while GOCART obviously underestimated dust emission over the GD (Fig. 9h). On 4 May, emitted dust from the GD was transported to the northeast China, and the highest AOD values for this case study were observed in the northern China (Fig. 9d). As the GD is the main dust source region of this dust storm, Shao2011 correctly captured the emission phase of this dust event.** ~~Extremely high AOD values were observed in the northern China from MODIS (Fig. 8a). When using GOCART dust emission scheme, AOD is highly underestimated over most regions except over Taklimakan Desert (Fig. 8b, 8c, 8d). When using Shao2011 dust emission scheme coupled with BS95 or PE92 dry deposition scheme (Fig. 8e, 8f, **8g**), AOD is also underestimated over most regions, but with relatively larger AOD than using GOCART dust emission scheme.~~ **Simulated AOD values from the S11Z01 configuration produced the closest**

match to the observed daily MODIS AOD with respect to the magnitude and spatial pattern~~AOD from the S11Z01 experiment is the closest one to the MODIS observed AOD~~ (Fig. **9n and Figure S3**). For a more quantitative comparison, ~~we collocated the simulated AOD with observed MODIS AOD over the 7-day simulation period 1-7 May, 2017.~~ Table ~~5~~ **6** shows the correlation coefficient (R) and root mean square error (RMSE) between the model and observed AOD for six experiments during 1-7 May. Overall, S11Z01 experiment gives a larger correlation coefficient and the RMSE is almost the same among different experiments, the correlation coefficient is still lower than 0.5. The low correlation may partly come from the spatial and temporal limitation of satellites and the difficulties to retrieve aerosol in the vicinity of clouds for satellites.

To evaluate the model performance in simulating the vertical profile of dust aerosol, we compared the extinction coefficient from model and from CALIPSO (Fig. 10). Figure 10 shows the Simulated and observed aerosol extinction profiles at 532 nm at 18:00 UTC 4 May. The trajectory of CALIPSO passes the East Asia (Fig. 10d). All the six experiments show the similar dust location in the atmosphere, which is consistent with the CALIPSO observation. However, the magnitude of dust concentration differs substantially. The simulated extinction coefficients using GOCART dust emission schemes are significantly underestimated compared to the CALIPSO observation (Fig. 10a,10b and 10c), while the modeled extinction coefficients using Shao2011 dust emission scheme agrees better with observation though they are still underestimated (Fig. 10e,10f and 10g). Among all the six experiments, results from S11Z01 agree the best with observation.

In summary, both ground and satellite observations indicate that the S11Z01 experiment yields the best performance in simulating this dust storm. As we discussed in Sect. 3.2, the Z01 dry deposition scheme indeed has a better physical treatment and performs better than some other dry deposition schemes.

~~3~~**4 Summary and discussion**

In this study, we analyzed the dust simulation sensitivity to different dust emission schemes and dry deposition schemes. In order to compare different dust emission schemes, the Shao2011 dust emission scheme has been implemented into the MOSAIC aerosol scheme in WRF-Chem v3.9. Six model experiments were conducted to simulate the dust storm in May 2017

over East Asia, with two dust emission schemes (GOCART and Shao2011) and three dry deposition schemes (BS95, PE92 and Z01). The simulation results of different experiments were evaluated against surface and satellite observations.

Our results show that dust loading is very sensitive to different dry deposition schemes. The relative difference of dust loading in different experiments range from 20%-116% when using different dry deposition schemes. The difference of dry deposition velocity in different dry deposition schemes comes from the parameterization of surface resistance, and difference in surface resistance mainly comes from the parameterization of collection efficiency from impaction and rebound effect. In addition, different dust emission schemes result in different spatial distribution of dust loading, as dust emission fluxes in dust source regions **differ substantially**~~differ a lot~~ among different dust emission schemes, which is mainly attributed to differences in the threshold conditions for dust emission and in formulas and parameters for calculating dust emission flux. We noted that, the Shao2011 dust emission scheme is different among different WRF-Chem versions, and **significant difference exist in the** simulated dust emission fluxes **between**~~in~~ WRF-Chem v3.9 and WRF-Chem v3.7.1~~ can differ a lot~~, which is mainly caused by differences in soil particle size distributions used in two versions (see Appendix B).

Compared with both surface PM_{10} station observations and MODIS AOD, the Shao2011 dust emission scheme coupled with the Z01 dry deposition scheme produces the best simulation for the dust storm in East Asia. **For PM10, S11Z01 experiment gives the largest R of 0.83 and the smallest RMSE of 82.98 of all the stations (Table 5). The spatial distribution of AOD during the simulation period obtained by S11Z01 agrees the best with MODIS AOD (Fig. 9), with the largest R and a relatively small RMSE (Table 6).** Our analysis indicates Z01 accounts for the rebound effect and E_{IM} changes with LUC and therefore has a better physical treatment of dry deposition velocity than the two other dry deposition schemes. Previous studies have also shown that the Z01 scheme agrees better with measured dry deposition fluxes and dry deposition velocity (e.g., Zhang et al., 2012; Connan et al, 2018). The Shao2011 dust emission scheme has larger dust emission fluxes than GOCART dust emission scheme over **the** Gobi Desert, and the transport of dust emitted from **the** Gobi Desert is the most important source of dust weather in northern China (Chen et al., 2017b). **Compared with daily MODIS AOD (Fig. 9), our results indicate that dust emission from Shao2011 is better for this dust event, in terms of dust spatial and temporal distributions.** ~~The Shao2011 scheme has also been documented to give better performance in dust simulation over East Asia (Su and Fung, 2015).~~ **We note that our results are obtained from simulations of a dust storm over a short period, and**

longer simulations are desirable in the future to test whether the optimal scheme here still produces best simulations.–

This study highlights the importance of dry deposition process in dust simulation. Future studies on dust simulation should pay attention to improve dry deposition schemes as well as the dust emission schemes. Additional field measurements of dry deposition process and comparisons with model results are required to reduce the uncertainties on dust simulation.

Appendix A: Description of the Shao2011 dust emission scheme

Here we describe the Shao2011 dust emission scheme in more detail as a supplement to the Sect. 2.2.2 of this article. The **total** saltation flux Q in Eq. (4) is calculated as:

$$Q = \int_{d_1}^{d_2} Q(d) p_m(d) \delta d \quad \textbf{(A1)}$$

where d_1 and d_2 define the upper and lower limits of saltation particle size. $p_m(d)$ is the the minimally disturbed particle-size distribution. The saltation flux Q for each particle size d is calculated as:

$$Q(d) = (1 - c_f) c_0 \frac{\rho_a}{g} u_*^3 \left(1 - \frac{u_{*t}}{u_*}\right)\left(1 + \frac{u_{*t}}{u_*}\right)^2 \quad \text{(A2)}$$

where c_f is the fraction of vegetation cover, (1-c_f) means the fraction of erodible surface area, c_0 is a coefficient. u_{*t} is the threshold friction velocity, u_* is the friction velocity. When u_* is larger than u_{*t}, it calculates the dust emission flux. Before WRF-Chem v4.0, there is a bug in calculating the saltation flux Q(d_s) in Shao2011. They miscalculate the last term as $(1+\left(\frac{u_{*t}}{u_*}\right)^2)$ in WRF-Chem codes (LeGrand et al., 2019). In WRF-Chem v4.0 and later versions, they fixed this bug and we also fixed this bug in our simulations.

The threshold friction velocity u_{*t} is calculated as:

$$u_{*t} = u_{*t0} f_\lambda f_\theta \quad \text{(A3)}$$

where u_{*t0} is the ideal threshold friction velocity when soil is dry, bare and free of crust and salt, f_λ is the correction functions for surface roughness, f_θ is the correction functions for soil moisture. The ideal threshold friction u_{*t0} is calculated as:

$$u_{*t0} = \sqrt{a_1 \frac{\rho_p}{\rho_a} g d + \frac{a_2}{\rho_a d}} \quad \text{(A4)}$$

where a_1 and a_2 are constant. ρ_p and ρ_a are particle and air density. d is the particle diameter.

The correction functions for surface roughness f_λ is calculated as:

$$f_\lambda = [(1 - m\sigma\lambda)(1 + m\beta_0\lambda)]^{\frac{1}{2}} \quad \text{(A5)}$$

where m is a constant, σ is the ratio of roughness-element basal area to frontal area, λ is the frontal area index, β_0 is the ratio of the drag coefficient of an isolated roughness element on the surface to the drag coefficient of the substrate surface itself.

The mass fraction of free dust η_{mi} is calculated as:

$$\eta_{mi} = \int_{d-\frac{\Delta d_i}{2}}^{d+\frac{\Delta d_i}{2}} p_m(d)\delta d \quad \text{(A6)}$$

where $p_m(d)$ is the minimally disturbed particle-size distribution, which is regarded as a composite of several log-normal distribution, $p_m(d)$ is expressed as:

$$p_m(d) = \frac{1}{d}\sum_{i=1}^{J} \frac{w_j}{\sqrt{2\pi}\sigma_j} exp\left(-\frac{(lnd - lnD_j)^2}{2\sigma_j^2}\right) \quad \text{(A7)}$$

soil samples collected from experiment sites are used to determine the particle size distribution.

Appendix B: The Shao2011 dust emission scheme in different versions of WRF-Chem

As we noted in Sect. 3.1, the Shao2011 scheme in different versions of WRF-Chem can produce significantly different dust emission fluxes. Here we document differences in Shao2011 among different WRF-Chem versions:

1. The first difference is c_0. c_0 is a coefficient used to calculate the saltation flux as in Eq. (A2). In versions before WRF-Chem v3.8, c_0 is equal to 0.5; in WRF-Chem v3.8 and later versions, c_0 is equal to 2.3 (Table B1).
2. The second difference is β_0. β_0 is a coefficient used to calculate the correction function for surface roughness f_λ in Eq. (A5). In versions before WRF-Chem v3.8, β_0~~β~~ is 90; in WRF-Chem v3.8 and later versions, β_0 ~~β~~ is 200 (Table B1).
3. The third difference is caused by the minimally disturbed particle-size distribution $p_m(d)$ (see Eq. (A6)). $p_m(d)$ is used to calculate the free dust fraction η_{mi} (see Eq. (A6)). Free dust fraction is the fraction of dust that has lower

enough binding energy so that it can be easily lifted from the surface by either aerodynamic forces or mechanical abrasion (Shao, 2001). The η_{mi} is used to calculate the dust emission rate in Eq. (4). 12 soil types are included in all WRF-Chem versions. In WRF-Chem v3.8 and later versions, each soil type has a corresponding $p_m(d)$ as listed in Table B1 from Shao et al. (2010); in versions before WRF-Chem v3.8, there are only four $p_m(d)$ as listed in Table 1 from Shao (2004) for 12 soil types (Fig. B1). For example, (f) sand and (g) loamy sand soil types use the same free dust fraction distribution in versions before WRF-Chem v3.8. As shown in Table B2, the loam and clay loam are the two soil types with the largest percentage, while the other soil types account for a very small percentage. From Fig. B1c and Fig. B1e, for loam and clay loam soil types, the free dust fraction is so small in the particle size range 0-10 um in WRF-Chem v3.8 and later versions, almost all close to 0; while in the versions before WRF-Chem v3.8, the free dust fraction is relatively high. In different WRF-Chem versions, the total saltation flux Q is the same, but dust emission flux $F(d_i)$ is different due to different free dust fraction (see Eq. (4)). With smaller free dust fraction, the dust emission flux is smaller in WRF-Chem v3.8 and later versions.

To examine the importance of these changes, we run four experiments to quantify the contribution of each factor (Table B3). For control run, c_0 is 2.3, β_0~~β~~ is 200 and $p_m(d)$ has 12 distributions based on WRF-Chem v3.8 or later versions. For case1 experiment, β_0~~β~~ is changed to 90, the one used in WRF-Chem v3.7.1 and all other parameters are kept the same as in control run. The dust emission of case1 is 1.35 times higher than the control run. For case2 experiment, c_0 is changed to 0.5, the one used in WRF-Chem v3.7.1, and all other parameters remain the same as in control run. The dust emission of case2 is twenty-one percent of the dust emission of the control run. For case3 experiment, $p_m(d)$ is adopted from WRF-Chem v3.7.1 and has four distributions, and all other parameters remain the same as in control run. The dust emission of case3 is 13 times higher than the control run. This indicates that the difference of dust emission between different versions of Shao2011 scheme is mainly caused by the change of $p_m(d)$. As $p_m(d)$ is determined by soil particle size distribution, this also highlights the need to improve the accuracy of soil texture.

We should mention that the Shao2011 dust emission scheme we used in this study is based on WRF-Chem v3.9 with the soil particle size distribution from WRF-Chem v3.7.1, which simulates better dust loading compared with observations. Compared with the original Shao2011 scheme in WRF-Chem v3.9, the total dust emission simulated in our experiments

during 1-7 May is 13 times higher.

Code availability

The source code of WRF-Chem is available at http://www2.mmm.ucar.edu/wrf/users/download/get_sources.html (last access: 31 October 2019). The modified WRF-Chem v3.9 with Shao2011 dust emission scheme implemented in MOSAIC aerosol scheme is available upon request to the corresponding author.

Data availability

The 6-hourly National Center for Environmental Prediction Final (NCEP/FNL) Operational Global Analysis data at a resolution of 1°×1° can be obtained from: https://rda.ucar.edu/ (last access: 31 October 2019). The observed PM10 data is collected from the National air quality real time release platform at: http://106.37.208.233:20035/ (last access: 31 October 2019). The historical data of air quality used in this study can be downloaded from: http://beijingair.sinaapp.com/ (last access: 31 October 2019). Daily MYD08_D3 files from the MODIS onboard Aqua satellite can be obtained from https://ladsweb.nascom.nasa.gov (last access: 31 October 2019).

Author contributions

MW and YZ conceived the idea and designed the model experiments. YZ performed the simulations, conducted the analysis and wrote the manuscript. CZ and SC provided guideline for the dust simulations in WRF-Chem and helped in the interpretation of the results. XH and ZL provided guideline for the WRF-Chem simulations and contributed to the model experiments design. YG helped in the PM10 data processing and usage. Everyone edited the manuscript.

Competing interests

The authors declare that they have no conflict of interest.

Acknowledgements

This work is supported by the Minister of Science and Technology of China (2016YFC0200503 and 2017YFA0604002) and by the National Natural Science Foundation of China (41575073, 41621005 and 91744208). This research is also supported by the Collaborative Innovation Center of Climate Change, Jiangsu Province. Chun Zhao is supported by the Natural Science Foundation of China NSFC (41775146) and the Fundamental Research Funds for the Central Universities.

References

Abuduwaili, J., LIU, D. and WU, G.: Saline dust storms and their ecological impacts in arid regions, J. Arid Land, 2(2), 144–150, doi:10.3724/sp.j.1227.2010.00144, 2010.

Bergametti, G., Marticorena, B., Rajot, J. L., Foret, G., Alfaro, S. C. and Laurent, B.: Size-Resolved Dry Deposition Velocities of Dust Particles: In Situ Measurements and Parameterizations Testing, J. Geophys. Res. Atmos., 123(19), 11,080-11,099, doi:10.1029/2018JD028964, 2018.

Binkowski, F. S. and Shankar, U.: The Regional Particulate Matter Model: 1. Model description and preliminary results, J. Geophys. Res., 100(D12), 26191, doi:10.1029/95JD02093, 1995.

Chamberlain, A. C.: Transport of Lycopodium spores and other small particles to rough surfaces, Proc. R. Soc. London. Ser. A. Math. Phys. Sci., 296(1444), 45–70, doi:10.1098/rspa.1967.0005, 1967.

Chen, F. and Dudhia, J.: Coupling an Advanced Land Surface–Hydrology Model with the Penn State–NCAR MM5 Modeling System. Part I: Model Implementation and Sensitivity, Mon. Weather Rev., 129(4), 569–585, doi:10.1175/1520-0493(2001)129<0569:CAALSH>2.0.CO;2, 2001.

Chen, S., Huang, J., Zhao, C., Qian, Y., Leung, L. R. and Yang, B.: Modeling the transport and radiative forcing of taklimakan dust over the tibetan plateau: A case study in the summer of 2006, J. Geophys. Res. Atmos., 118(2), 797–812, doi:10.1002/jgrd.50122, 2013.

Chen, S., Huang, J., Qian, Y., Zhao, C., Kang, L., Yang, B. and Wang, Y.: An Overview of Mineral Dust Modeling over East Asia, , 31(August), doi:10.1007/s13351-017-6142-2.1.Introduction, 2017a.

Chen, S., Huang, J., Kang, L., Wang, H., Ma, X., He, Y., Yuan, T., Yang, B., Huang, Z. and Zhang, G.: Emission, transport, and radiative effects of mineral dust from the Taklimakan and Gobi deserts: Comparison of measurements and model results, Atmos. Chem. Phys., 17(3), 2401–2421, doi:10.5194/acp-17-2401-2017, 2017b.

Chen, S., Zhang, X., Lin, J., Huang, J., Zhao, D., Yuan, T., Huang, K., Luo, Y., Jia, Z., Zang, Z., Qiu, Y. and Xie, L.: Fugitive Road Dust PM2.5 Emissions and Their Potential Health Impacts, Environ. Sci. Technol., 53, 8455–8465, doi:10.1021/acs.est.9b00666, 2019.

Connan, O., Pellerin, G., Maro, D., Damay, P., Hébert, D., Roupsard, P., Rozet, M. and Laguionie, P.: Dry deposition velocities of particles on grass : Field experimental data and comparison with models, J. Aerosol Sci., 126(July), 58–67, doi:10.1016/j.jaerosci.2018.08.004, 2018.

Creamean, J. M., Suski, K. J., Rosenfeld, D., Cazorla, A., Demott, P. J., Sullivan, R. C., White, A. B., Ralph, F. M., Minnis, P., Comstock, J. M., Tomlinson, J. M. and Prather, K. A.: Dust and Biological Aerosols, , 339(March), 1572–1579, 2013.

Demott, P. J., Prenni, A. J., Liu, X., Kreidenweis, S. M., Petters, M. D., Twohy, C. H. and Richardson, M. S.: Predicting global atmospheric ice nuclei distributions and their impacts on climate, , 1–6, doi:10.1073/pnas.0910818107, 2010.

Gallagher, M. W.: Measurements and parameterizations of small aerosol deposition velocities to grassland, arable crops, and forest: Influence of surface roughness length on deposition, J. Geophys. Res., 107(D12), 4154, doi:10.1029/2001JD000817, 2002.

Giardina, M. and Buffa, P.: A new approach for modeling dry deposition velocity of particles, Atmos. Environ., 180(September 2017), 11–22, doi:10.1016/j.atmosenv.2018.02.038, 2018.

Ginoux, P., Chin, M., Tegen, I., Prospero, J. M., Holben, B., Dubovik, O. and Lin, S.-J.: Sources and distributions of dust aerosols simulated with the GOCART model, J. Geophys. Res. Atmos., 106(D17), 20255–20273, doi:10.1029/2000JD000053, 2001.

Giorgi, F.: A particle dry-deposition parameterization scheme for use in tracer transport models, J. Geophys. Res., 91(D9), 9794, doi:10.1029/JD091iD09p09794, 1986.

Giorgi, F.: Dry deposition velocities of atmospheric aerosols as inferred by applying a particle dry deposition parameterization to a general circulation model, Tellus B, 40B(1), 23–41, doi:10.1111/j.1600-0889.1988.tb00210.x, 1988.

Grell, G. A. and Freitas, S. R.: A scale and aerosol aware stochastic convective parameterization for weather and air quality modeling, Atmos. Chem. Phys., 14(10), 5233–5250, doi:10.5194/acp-14-5233-2014, 2014.

Grell, G. A., Peckham, S. E., Schmitz, R., McKeen, S. A., Frost, G., Skamarock, W. C. and Eder, B.: Fully coupled “online” chemistry within the WRF model, Atmos. Environ., 39(37), 6957–6975, doi:10.1016/j.atmosenv.2005.04.027, 2005.

Guo, P., Yu, S., Wang, L., Li, P., Li, Z., Mehmood, K., Chen, X., Liu, W., Zhu, Y., Yu, X., Alapaty, K., Lichtfouse, E.,

Rosenfeld, D. and Seinfeld, J. H.: High-altitude and long-range transport of aerosols causing regional severe haze during extreme dust storms explains why afforestation does not prevent storms, Environ. Chem. Lett., 1–8, doi:10.1007/s10311-019-00858-0, 2019.

Hansen, J., Sato, M. and Ruedy, R.: Radiative forcing and climate response, J. Geophys. Res. Atmos., 102(D6), 6831–6864, doi:10.1029/96JD03436, 1997.

Hicks, B. B., Saylor, R. D. and Baker, B. D.: Dry deposition of particles to canopies-A look back and the road forward, J. Geophys. Res. Atmos., 121(24), 14,691-14,707, doi:10.1002/2015JD024742, 2016.

Hofer, J., Althausen, D., Abdullaev, S. F., Makhmudov, A. N., Nazarov, B. I., Schettler, G., Engelmann, R., Baars, H., Fomba, K. W., Müller, K., Heinold, B., Kandler, K. and Ansmann, A.: Long-term profiling of mineral dust and pollution aerosol with multiwavelength polarization Raman lidar at the Central Asian site of Dushanbe, Tajikistan: Case studies, Atmos. Chem. Phys., 17(23), 14559–14577, doi:10.5194/acp-17-14559-2017, 2017.

Hong, S.-Y., Noh, Y. and Dudhia, J.: A New Vertical Diffusion Package with an Explicit Treatment of Entrainment Processes, Mon. Weather Rev., 134(9), 2318–2341, doi:10.1175/MWR3199.1, 2006.

Huneeus, N., Schulz, M., Balkanski, Y., Griesfeller, J., Prospero, J., Kinne, S., Bauer, S., Boucher, O., Chin, M., Dentener, F., Diehl, T., Easter, R., Fillmore, D., Ghan, S., Ginoux, P., Grini, A., Horowitz, L., Koch, D., Krol, M. C., Landing, W., Liu, X., Mahowald, N., Miller, R., Morcrette, J.-J., Myhre, G., Penner, J., Perlwitz, J., Stier, P., Takemura, T. and Zender, C. S.: Global dust model intercomparison in AeroCom phase I, Atmos. Chem. Phys., 11(15), 7781–7816, doi:10.5194/acp-11-7781-2011, 2011.

Iacono, M. J., Delamere, J. S., Mlawer, E. J., Shephard, M. W., Clough, S. A. and Collins, W. D.: Radiative forcing by long-lived greenhouse gases: Calculations with the AER radiative transfer models, J. Geophys. Res. Atmos., 113(13), 2–9, doi:10.1029/2008JD009944, 2008.

Jiménez-Guerrero, P., Pérez, C., Jorba, O. and Baldasano, J. M.: Contribution of Saharan dust in an integrated air quality system and its on-line assessment, Geophys. Res. Lett., 35(3), 1–6, doi:10.1029/2007GL031580, 2008.

Kang, J. Y., Yoon, S. C., Shao, Y. and Kim, S. W.: Comparison of vertical dust flux by implementing three dust emission schemes in WRF / Chem, , 116(May), 1–18, doi:10.1029/2010JD014649, 2011.

Khan, T. R. and Perlinger, J. A.: Evaluation of five dry particle deposition parameterizations for incorporation into atmospheric transport models, Geosci. Model Dev., 10(10), 3861–3888, doi:10.5194/gmd-10-3861-2017, 2017.

Kok, J. F.: A scaling theory for the size distribution of emitted dust aerosols suggests climate models underestimate the size of the global dust cycle, Proc. Natl. Acad. Sci. U. S. A., 108(3), 1016–1021, doi:10.1073/pnas.1014798108, 2011.

Kok, J. F., Ridley, D. A., Zhou, Q., Miller, R. L., Zhao, C., Heald, C. L., Ward, D. S., Albani, S. and Haustein, K.: Smaller desert dust cooling effect estimated from analysis of dust size and abundance, , doi:10.1038/NGEO2912, 2017.

LeGrand, S. L., Polashenski, C., Letcher, T. W., Creighton, G. A., Peckham, S. E. and Cetola, J. D.: The AFWA dust emission

scheme for the GOCART aerosol model in WRF-Chem v3.8.1, Geosci. Model Dev., 12(1), 131–166, doi:10.5194/gmd-12-131-2019, 2019.

Marticorena, B. and Bergametti, G.: Modeling the atmospheric dust cycle: 1. Design of a soil-derived dust emission scheme, J. Geophys. Res., 100(D8), 16415, doi:10.1029/95JD00690, 1995.

Morrison, H., Thompson, G. and Tatarskii, V.: Impact of Cloud Microphysics on the Development of Trailing Stratiform Precipitation in a Simulated Squall Line: Comparison of One- and Two-Moment Schemes, Mon. Weather Rev., 137(3), 991–1007, doi:10.1175/2008mwr2556.1, 2008.

Ozer, P., Laghdaf, M. B. O. M., Lemine, S. O. M. and Gassani, J.: Estimation of air quality degradation due to Saharan dust at Nouakchott, Mauritania, from horizontal visibility data, Water. Air. Soil Pollut., 178(1–4), 79–87, doi:10.1007/s11270-006-9152-8, 2007.

Peters, K. and Eiden, R.: Modelling the dry deposition velocity of aerosol particles to a spruce forest, Atmos. Environ. Part A. Gen. Top., 26(14), 2555–2564, doi:10.1016/0960-1686(92)90108-W, 1992.

Petroff, A. and Zhang, L.: Development and validation of a size-resolved particle dry deposition scheme for application in aerosol transport models, Geosci. Model Dev., 3(2), 753–769, doi:10.5194/gmd-3-753-2010, 2010.

Petroff, A., Mailliat, A., Amielh, M. and Anselmet, F.: Aerosol dry deposition on vegetative canopies. Part I: Review of present knowledge, Atmos. Environ., 42(16), 3625–3653, doi:10.1016/j.atmosenv.2007.09.043, 2008.

Prospero, J. M., Landing, W. M. and Schulz, M.: African dust deposition to Florida: Temporal and spatial variability and comparisons to models, J. Geophys. Res., 115(D13), D13304, doi:10.1029/2009JD012773, 2010.

Pryor, S. C., Gallagher, M., Sievering, H., Larsen, S. E., Barthelmie, R. J., Birsan, F., Nemitz, E., Rinne, J., Kulmala, M., Grönholm, T., Taipale, R. and Vesala, T.: A review of measurement and modelling results of particle atmosphere–surface exchange, Tellus B Chem. Phys. Meteorol., 60(1), 42–75, doi:10.1111/j.1600-0889.2007.00298.x, 2008.

Ruijrok, W., Davidson, C. I. and Nicholson, K. W.: Dry deposition of particles, Tellus B Chem. Phys. Meteorol., 47(5), 587–601, doi:10.3402/tellusb.v47i5.16074, 1995.

Seinfeld, J. H. and Pandis, S. N.: ATMOSPHERIC From Air Pollution to Climate Change SECOND EDITION., 2006.

Shao, Y.: A model for mineral dust emission, J. Geophys. Res. Atmos., 106(D17), 20239–20254, doi:10.1029/2001JD900171, 2001.

Shao, Y.: Simplification of a dust emission scheme and comparison with data, J. Geophys. Res. D Atmos., 109(10), 1–6, doi:10.1029/2003JD004372, 2004.

Shao, Y., Fink, A. H. and Klose, M.: Numerical simulation of a continental-scale Saharan dust event, J. Geophys. Res., 115(D13), D13205, doi:10.1029/2009JD012678, 2010.

Shao, Y., Ishizuka, M., Mikami, M. and Leys, J. F.: Parameterization of size-resolved dust emission and validation with measurements, J. Geophys. Res., 116(D8), D08203, doi:10.1029/2010JD014527, 2011.

Slinn, W. G. .: Predictions for particle deposition to vegetative canopies, Atmos. Environ., 16(7), 1785–1794, doi:10.1016/0004-6981(82)90271-2, 1982.

Su, L. and Fung, J. C. H.: Sensitivities of WRF-Chem to dust emission schemes and land surface properties in simulating dust cycles during springtime over East Asia, J. Geophys. Res. Atmos., 120(21), 11,215-11,230, doi:10.1002/2015JD023446, 2015.

Todd, M. C., Bou Karam, D., Cavazos, C., Bouet, C., Heinold, B., Baldasano, J. M., Cautenet, G., Koren, I., Perez, C., Solmon, F., Tegen, I., Tulet, P., Washington, R. and Zakey, A.: Quantifying uncertainty in estimates of mineral dust flux: An intercomparison of model performance over the Bodélé Depression, northern Chad, J. Geophys. Res., 113(D24), D24107, doi:10.1029/2008JD010476, 2008.

Uno, I., Wang, Z., Chiba, M., Chun, Y. S., Gong, S. L., Hara, Y., Jung, E., Lee, S.-S., Liu, M., Mikami, M., Music, S., Nickovic, S., Satake, S., Shao, Y., Song, Z., Sugimoto, N., Tanaka, T. and Westphal, D. L.: Dust model intercomparison (DMIP) study over Asia: Overview, J. Geophys. Res., 111(D12), D12213, doi:10.1029/2005JD006575, 2006.

Wesely, M. L., Cook, D. R. and Hart, R. L.: Measurements and parameterization of particulate sulfur dry deposition over grass, J. Geophys. Res., 90(4), 2131–2143, 1985.

Wu, C.-L. and Lin, Z.-H.: Uncertainty in Dust Budget over East Asia Simulated by WRF/Chem with Six Different Dust Emission Schemes, Atmos. Ocean. Sci. Lett., 6(6), 428–433, doi:10.1080/16742834.2013.11447120, 2013.

Wu, C.-L. and Lin, Z.-H.: Impact of two different dust emission schemes on the simulation of a severe dust storm in East Asia using the WRF/Chem model, Clim. Environ. Res. (in Chinese), 19(4), 419–436, doi:10.3878/j.issn.1006-9585.2013.13041, 2014.

Wu, M., Liu, X., Zhang, L., Wu, C., Lu, Z., Ma, P. L., Wang, H., Tilmes, S., Mahowald, N., Matsui, H. and Easter, R. C.: Impacts of Aerosol Dry Deposition on Black Carbon Spatial Distributions and Radiative Effects in the Community Atmosphere Model CAM5, J. Adv. Model. Earth Syst., 10(5), 1150–1171, doi:10.1029/2017MS001219, 2018.

Yuan, T., Chen, S., Huang, J., Zhang, X., Luo, Y., Ma, X. and Zhang, G.: Sensitivity of simulating a dust storm over Central Asia to different dust schemes using the WRF-Chem model, Atmos. Environ., 207(March), 16–29, doi:10.1016/j.atmosenv.2019.03.014, 2019.

Zaveri, R. A. and Peters, L. K.: A new lumped structure photochemical mechanism for large-scale applications, J. Geophys. Res. Atmos., 104(D23), 30387–30415, doi:10.1029/1999JD900876, 1999.

Zaveri, R. A., Easter, R. C., Fast, J. D. and Peters, L. K.: Model for Simulating Aerosol Interactions and Chemistry (MOSAIC), J. Geophys. Res. Atmos., 113(13), 1–29, doi:10.1029/2007JD008782, 2008.

Zender, C. S., Miller, R. L. R. L. and Tegen, I.: Quantifying mineral dust mass budgets:Terminology, constraints, and current estimates, Eos, Trans. Am. Geophys. Union, 85(48), 509–512, doi:10.1029/2004EO480002, 2004.

Zhang, J. and Shao, Y.: A new parameterization of particle dry deposition over rough surfaces, Atmos. Chem. Phys., 14(22), 12429–12440, doi:10.5194/acp-14-12429-2014, 2014.

Zhang, L. and He, Z.: Technical Note: An empirical algorithm estimating dry deposition velocity of fine, coarse and giant particles, Atmos. Chem. Phys., 14(7), 3729–3737, doi:10.5194/acp-14-3729-2014, 2014.

Zhang, L., Gong, S., Padro, J. and Barrie, L.: A size-segregated particle dry deposition scheme for an atmospheric aerosol module, Atmos. Environ., 35(3), 549–560, doi:10.1016/S1352-2310(00)00326-5, 2001.

Zhang, L., Fang, G. C., Liu, C. K., Huang, Y. L., Huang, J. H. and Huang, C. S.: Dry deposition fluxes and deposition velocities of seven trace metal species at five sites in central Taiwan - A summary of surrogate surface measurements and a comparison with model estimations, Atmos. Chem. Phys., 12(7), 3405–3417, doi:10.5194/acp-12-3405-2012, 2012.

Zhang, X., Sharratt, B., Liu, L., Wang, Z., Pan, X., Lei, J., Wu, S., Huang, S.-Y., Guo, Y.-H., Li, J., Tang, X., Yang, T., Tian, Y., Chen, X.-S., Hao, J.-Q., Zheng, H.-T., Yang, Y.-Y. and Lyu, Y.-L.: East Asian dust storm in May 2017: observations, modelling, and its influence on the Asia-Pacific region, Atmos. Chem. Phys., 18(11), 8353–8371, doi:10.5194/acp-18-8353-2018, 2018.

Zhang, X. X., Sharratt, B., Lei, J. Q., Wu, C. L., Zhang, J., Zhao, C., Wang, Z. F., Wu, S. X., Li, S. Y., Liu, L. Y., Huang, S. Y., Guo, Y. H., Mao, R., Li, J., Tang, X. and Hao, J. Q.: Parameterization schemes on dust deposition in northwest China: Model validation and implications for the global dust cycle, Atmos. Environ., 209(April), 1–13, doi:10.1016/j.atmosenv.2019.04.017, 2019.

Zhao, C., Liu, X., Leung, L. R., Johnson, B., McFarlane, S. A., Gustafson, W. I., Fast, J. D. and Easter, R.: The spatial distribution of mineral dust and its shortwave radiative forcing over North Africa: Modeling sensitivities to dust emissions and aerosol size treatments, Atmos. Chem. Phys., 10(18), 8821–8838, doi:10.5194/acp-10-8821-2010, 2010.

Zhao, C., Liu, X., Leung, L. R. and Hagos, S.: Radiative impact of mineral dust on monsoon precipitation variability over West Africa, Atmos. Chem. Phys., 11(5), 1879–1893, doi:10.5194/acp-11-1879-2011, 2011.

Zhao, C., Liu, X. and Leung, L. R.: Impact of the Desert dust on the summer monsoon system over Southwestern North America, Atmos. Chem. Phys., 12(8), 3717–3731, doi:10.5194/acp-12-3717-2012, 2012.

Zhao, C., Chen, S., Leung, L. R., Qian, Y., Kok, J. F., Zaveri, R. A. and Huang, J.: Uncertainty in modeling dust mass balance and radiative forcing from size parameterization, Atmos. Chem. Phys., 13(21), 10733–10753, doi:10.5194/acp-13-10733-2013, 2013.

Zhao, T. L., Gong, S. L., Zhang, X. Y., Abdel-Mawgoud, A. and Shao, Y. P.: An assessment of dust emission schemes in modeling east Asian dust storms, J. Geophys. Res. Atmos., 111(5), 1–11, doi:10.1029/2004JD005746, 2006.

Table 1. WRF-Chem configuration

Atmospheric Process	WRF-Chem option	Namelist Variable	Option
Surface Layer physics	Noah land-surface model	sf_surface_physics	2
Soil map	**USGS**	**num_land_cat**	**24**
Boundary Layer Physics	YSU scheme	bl_pbl_physics	1
Longwave/Shortwave Radiation	RRTMG	ra_lw(sw)_physics	4
Cumulus Clouds	Grell-Freitas	cu_physics	3
Cloud microphysics	Morrison double-moment	mp_physics	10
Gas-phase/aerosol chemistry	CBMZ/MOSAIC 4-bin	chem_opt	9

Table 2. Three dry deposition schemes

Scheme	BS95	PE92	Z01
V_d	$V_d = V_g + \frac{1}{R_a + R_s + R_a R_S V_g}$	$V_d = V_g + \frac{1}{R_a + R_S}$	$V_d = V_g + \frac{1}{R_a + R_s + R_a R_S V_g}$
R_S	$R_s = \frac{1}{u_*(E_B + E_{IM})}$	$R_s = \frac{1}{u_*(E_B + E_{IM} + E_{IN})R}$	$R_s = \frac{1}{\varepsilon_0 u_*(E_B + E_{IM} + E_{IN})R}$
E_{IM}	$E_{IM} = 10^{-St}$	$E_{IM} = \left(\frac{St}{0.8 + St}\right)^2$	$E_{IM} = \left(\frac{St}{\alpha + St}\right)^{\beta}$
E_{IN}	0	$E_{IN} = \frac{(0.0016 + 0.0061 z_0) d_p}{1.414 \times 10^{-7}}$	$E_{IN} = \frac{1}{2}\left(\frac{d_p}{A}\right)^2$
R	1.0	$R_1 = e^{-2\sqrt{St}}$	$e^{-1.0\sqrt{St}}$
St	$St = \frac{u_*^2 v_g}{g\nu}$	$St = \frac{\rho_p d_p^2}{9\mu d_c} u$	$St = \frac{v_g u_*}{gA}$(vegetated surfaces) $St = \frac{v_g u_*^2}{g\nu}$(smooth surfaces)

Table 3. Model experiments and the corresponding model configuration in WRF-Chem. ~~Note that the dust_opt =15 option for Shao2011 is added to WRF-Chem by ourselves.~~

Experiment name	Dust emission scheme	Dry deposition scheme	**aer_drydep_opt**
GOBS95	GOCART	BS95	**1**
GOPE92	GOCART	PE92	**101**
GOZ01	GOCART	Z01	**301**
S11BS95	Shao2011	BS95	**1**
S11PE92	Shao2011	PE92	**101**
S11Z01	Shao2011	Z01	**301**

Table 4. Correlation coefficient (R) and root mean square error (RMSE) between WRF-Chem simulation and FNL reanalysis data for daily mean temperature at 2 meters, U component of wind, V component of wind and wind speed at 10 meters during the dust event time period. The last two rows show the R and RMSE for the time-averaged temperature at 2 meters, U component of wind, V component of wind and wind speed at 10 meters from 1 May to 2 May.

Day	R/RMSE	Temperature	U	V	Wind speed
1 May	R	0.99	0.86	0.85	0.75
1 May	RMSE	1.32	1.51	1.59	1.60
2 May	R	0.99	0.90	0.88	0.82
2 May	RMSE	1.28	1.61	1.60	1.70
3 May	R	1.0	0.91	0.90	0.84
3 May	RMSE	1.22	1.60	1.64	1.76
4 May	R	0.99	0.87	0.87	0.78
4 May	RMSE	1.35	1.57	1.49	1.63
5 May	R	0.99	0.88	0.87	0.80
5 May	RMSE	1.23	1.49	1.44	1.57
6 May	R	0.99	0.88	0.87	0.80
6 May	RMSE	1.32	1.56	1.52	1.63
7 May	R	0.99	0.89	0.82	0.79
7 May	RMSE	1.37	1.42	1.30	1.39
1 May to 7 May	R	1.0	0.90	0.86	0.82
1 May to 7 May	RMSE	1.03	1.08	0.98	1.11

840

Table 5. Correlation coefficient (R) and root mean square error (RMSE) between the model and observations for PM_{10} over five sub regions and **for all the stations** over whole China in Fig. ~~6~~ **7** for six experiments listed in Table 3.

Region	R/RMSE	GOBS95	GOPE92	GOZ01	S11BS95	S11PE92	S11Z01
TD	R	0.64	0.53	0.59	0.34	0.37	0.37
TD	RMSE	79.61	91.91	106.61	124.25	119.54	115.68
GD	R	0.75	0.78	0.82	0.76	0.75	0.74
GD	RMSE	174.81	137.14	77.81	193.23	128.21	82.58
NCP	R	0.75	0.73	0.73	0.78	0.76	0.77
NCP	RMSE	231.2	221.05	197.43	189.08	164.25	107.20
NEP	R	0.62	0.63	0.58	0.70	0.68	0.68
NEP	RMSE	177.17	174.52	171.96	159.47	144.77	126.91
YR	R	0.45	0.42	0.43	0.67	0.61	0.61
YR	RMSE	105.96	105.97	93.97	94.07	93.79	69.94
Total	R	0.50	0.60	0.63	0.85	0.83	0.83
Total	RMSE	146.58	137.96	120.57	133.71	113.88	82.98

845

Table 6. Correlation coefficient (R) and root mean square error (RMSE) between the model and MODIS observation for AOD for six experiments over the 7-day simulation period 1-7 May, 2017.

	GOBS95	GOPE92	GOZ01	S11BS95	S11PE92	S11Z01
R	0.32	0.37	0.35	0.40	0.39	0.42
RMSE	0.46	0.46	0.46	0.46	0.47	0.47

Table B1. Differences in Shao2011 dust emission scheme between different WRF-Chem versions

	Before WRF-Chem v3.8	WRF-Chem v3.8 and later
c_0	0.5	2.3
β_0	90	200
η_{mi}	~~/~~**4 types**	~~/~~**12 types**

Table B2. Percentage of each soil type in the whole East Asia domain

Soil type	Sand	Loamy sand	Sandy loam	Silt loam	silt	loam
percentage	2.6%	0.2%	4.0%	9.3%	0	47.6%
Soil type	Sandy clay loam	Silty clay loam	Clay loam	Sandy clay	Silty clay	clay
percentage	8.6%	0	21.7%	0	0.05%	6.0%

Table B3. Sensitivity of the simulated total dust emission from the Shao2011 to model parameters over the 7-day simulation period 1-7 May, 2017. The multiple of the dust emission of different cases is calculated with respect to the control run.

	C_0	β_0	η_{mi}	Dust emission (Tg)	Multiple
control run	2.3	200	12 types	1.35	1.00
case1	2.3	90	12 types	1.83	1.35
case2	0.5	200	12 types	0.29	0.21
case3	2.3	200	4 types	17.5	13.00

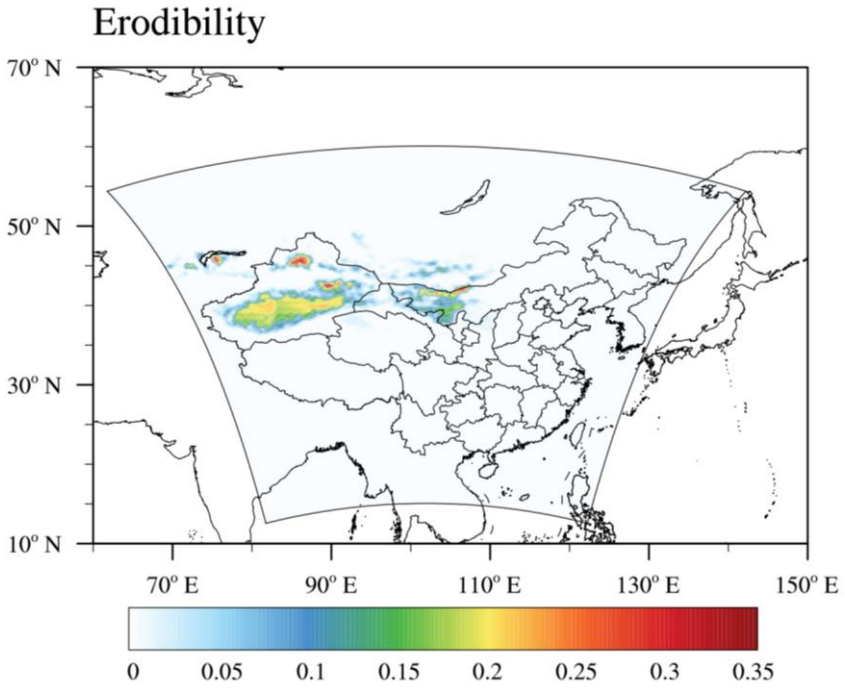

Figure 1. Domain map for the WRF-Chem simulations. The color shading shows the erodibility factor which is the fraction of erodible surface in each grid cell.

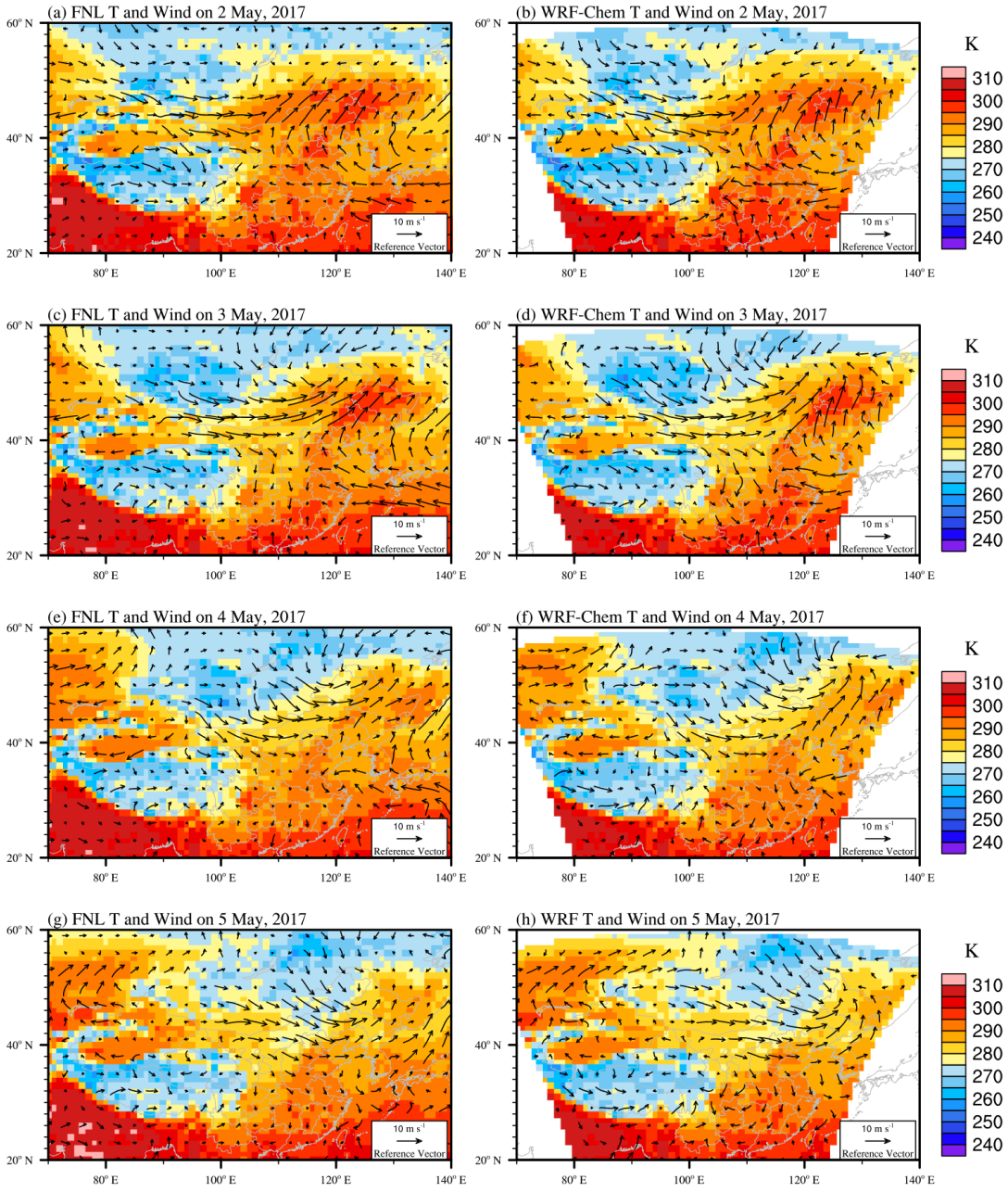

Figure 2. The surface meteorological conditions during the dust event. The color contours show the daily mean temperature field at 2 meters. Vectors represent the daily mean wind field at 10 meters. Panels (a)(c)(e)(g) show the NCEP/FNL reanalysis data. Panels (b)(d)(f)(h) show the WRF-Chem simulation.

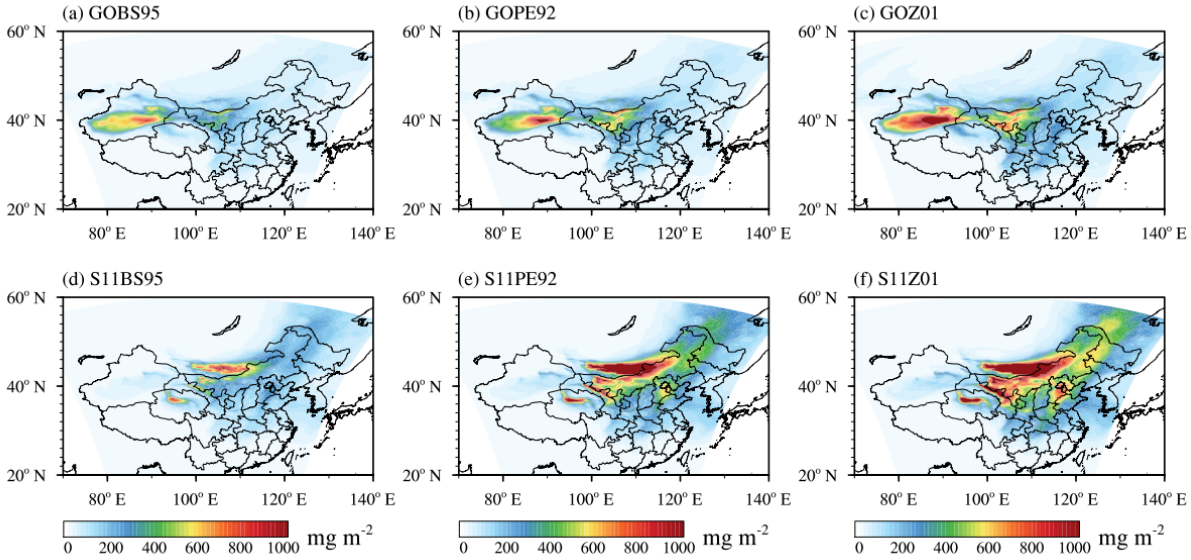

Figure 3. Spatial distribution of simulated mean dust loading for six experiments (a)GOBS95, (b)GOPE92, (c)GOZ01, (d)S11BS95, (e)S11PE92, (f)S11Z01 over the 7-day simulation period from 00:00 UTC on 1 May to 23:00 UTC on 7 May, 2017 (unit: mg m^{-2}).

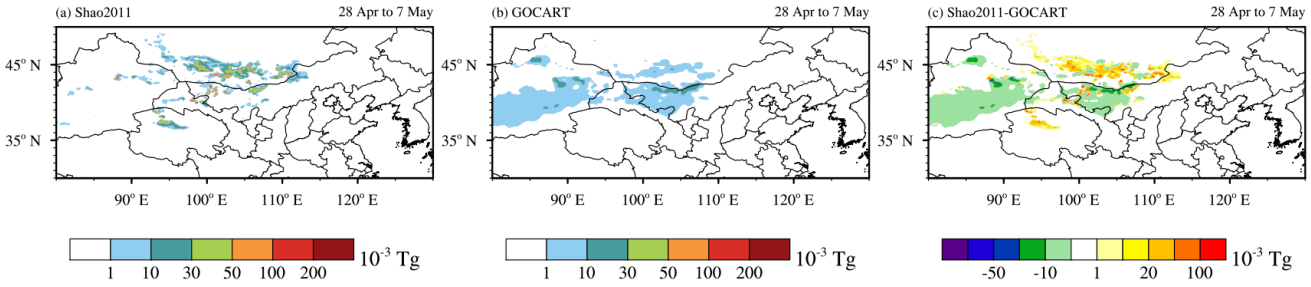

955

Figure 4. The simulated total dust emission (10^{-3} Tg) from two dust emission schemes: (a) Shao2011 and (b) GOCART from 00:00 UTC on 28 April to 23:00 UTC on 7 May, 2017. (c) The total dust emission flux difference between Shao2011 and GOCART. The diameter of the emitted dust is less than 10 μm in both GOCART and Shao2011 dust emission schemes.

960

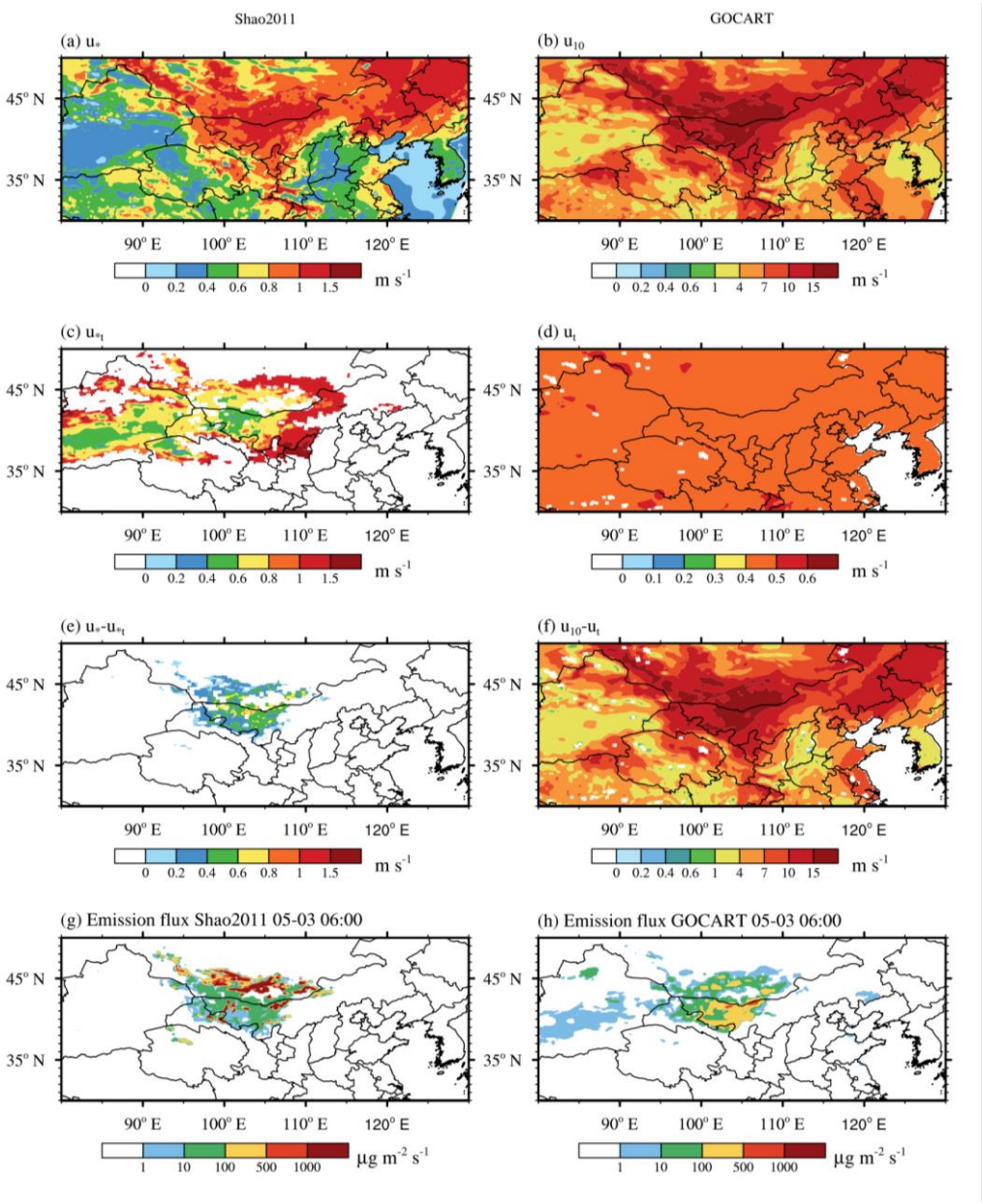

Figure 5. Spatial distribution of (a) friction velocity (u_*), (c) threshold friction velocity (u_{*t}) and (e) the difference between u_* and u_{*t} ($u_* - u_{*t}$) from Shao2011 dust emission scheme at 06:00 UTC on 3 May, 2017; (b) wind speed at 10 meters (u_{10}), (d) threshold velocity (u_t) and the difference between u_{10} and u_t ($u_{10} - u_t$) from GOCART dust emission scheme at 06:00 UTC on 3 May, 2017. Spatial distribution of (g) dust emission flux from Shao2011, (h) dust emission flux from GOCART at 06:00 UTC on 3 May, 2017.

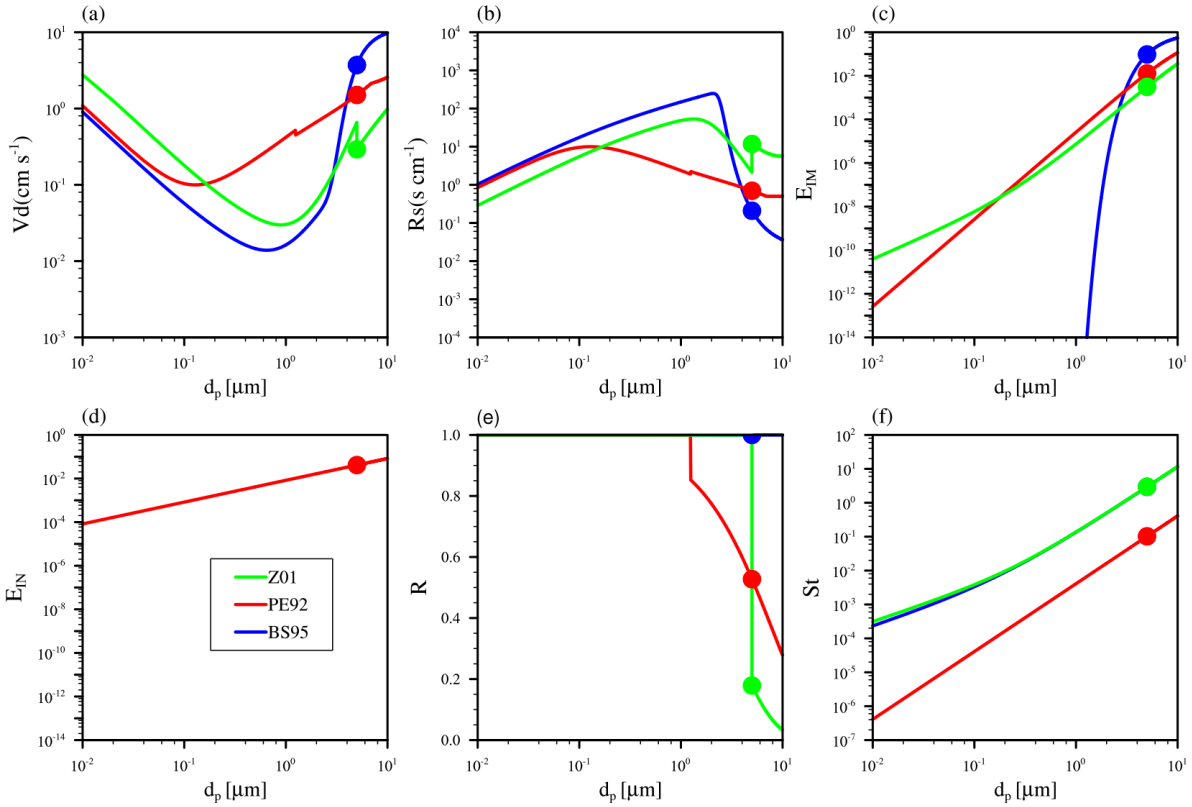

970

Figure 6. (a) Dry deposition velocity (V_d), (b) surface resistance (R_S), (c) surface collection efficiency from impaction (E_{IM}), (d) surface collection efficiency from interception (E_{IN}), (e) rebound (R) and (f) stokes number (St) as a function of particle diameter (~~Dp~~d_p) over desert surface computed using different dry deposition schemes (BS95, PE92 and Z01). The colored dots indicate at the reference diameter of 5 µm.

975

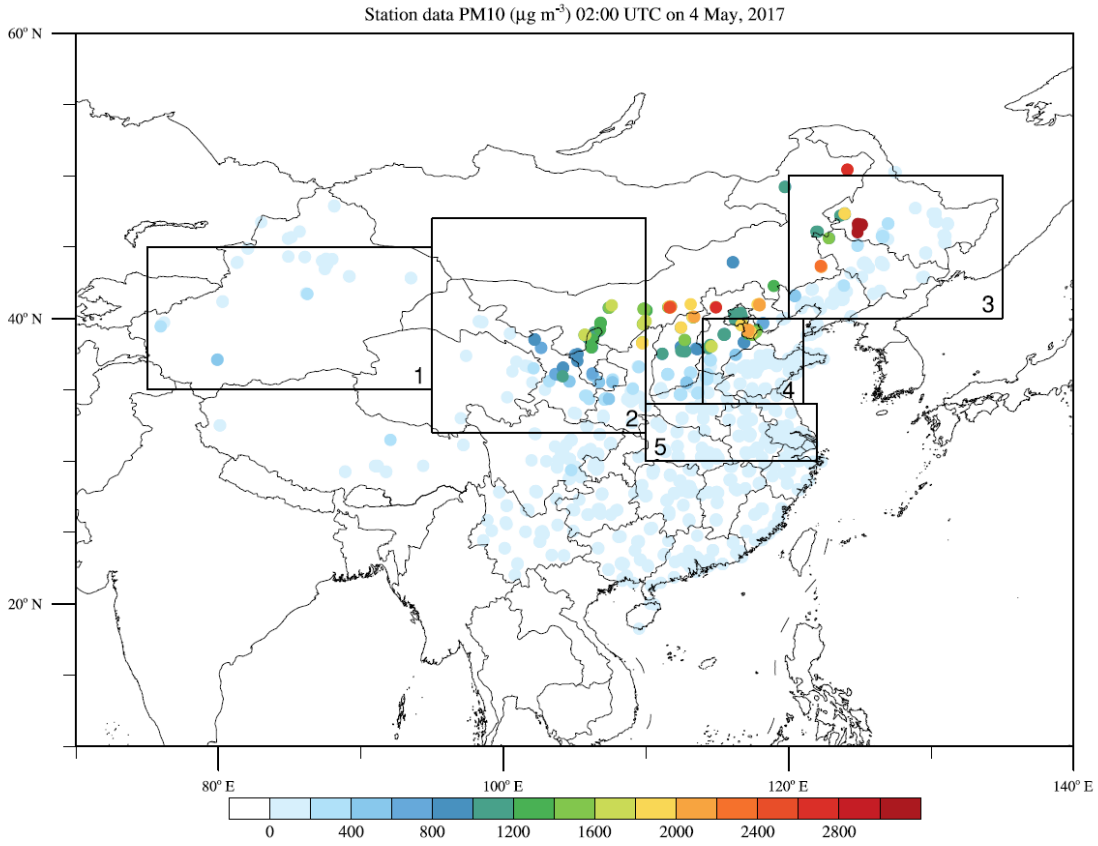

Figure 7. Five sub regions and observed PM_{10} concentrations. "1" represents **the** Taklimakan Desert (TD), "2" represents **the** Gobi Desert (GD), "3" represents **the** Northeastern plain (NEP), "4" represents **the** North China Plain (NCP), "5" represents **the** Middle and lower reaches of Yangtze River Plain (YR). The colored dots represent observed PM_{10} concentrations over observational sites at 02:00 UTC on 4 May, 2017 (10:00 Beijing Time (BJT) on 4 May, 2017).

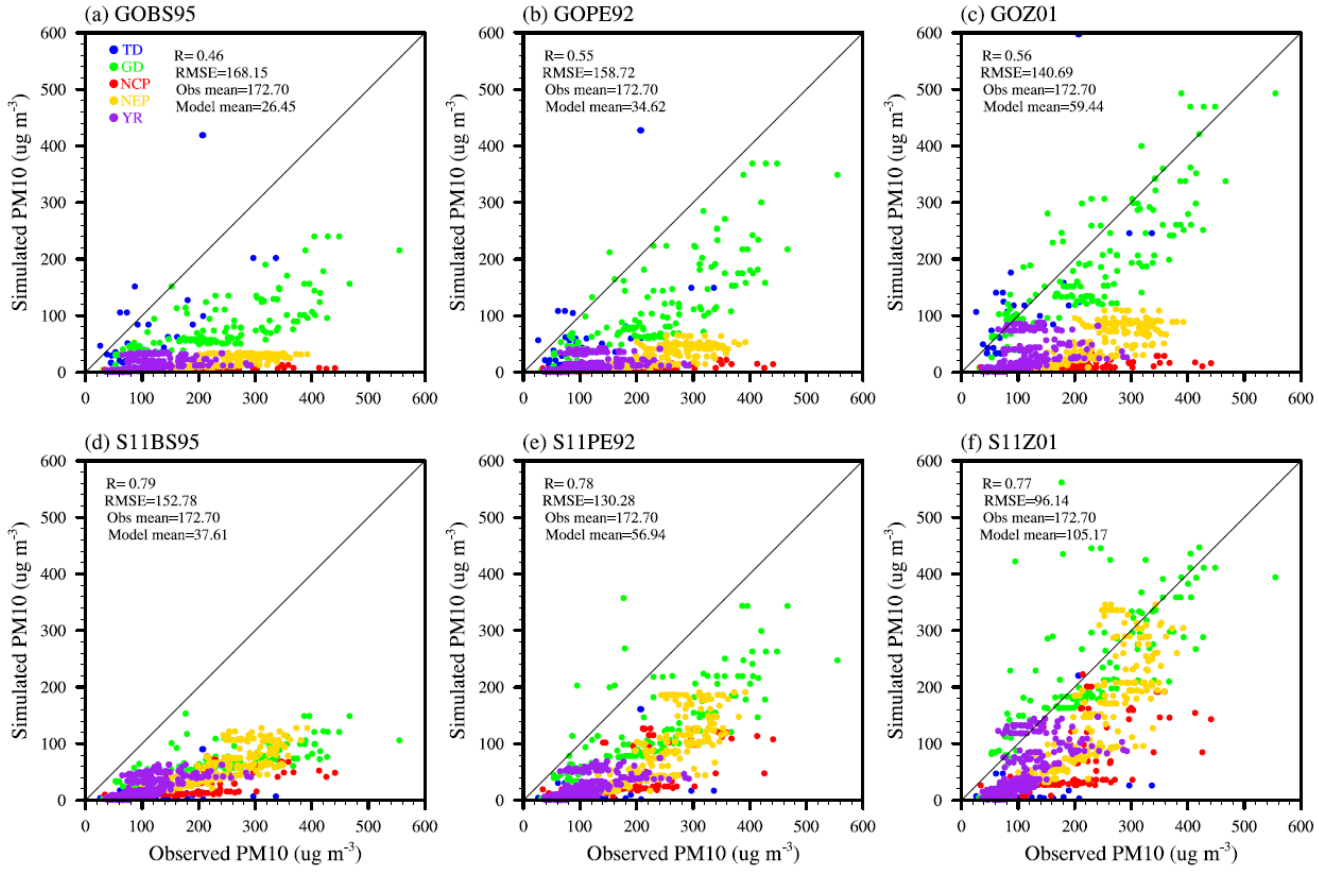

985 **Figure 8.** Simulated PM_{10} versus observed PM_{10} for six experiments (a)GOBS95, (b)GOPE92, (c)GOZ01, (d)S11BS95, (e)S11PE92, (f)S11Z01 over the 7-day simulation period 1-7 May, 2017. "Obs mean" is mean PM_{10} **over 1-7 May** from observation, "Model mean" is mean PM_{10} **over 1-7 May** from simulation, "R" is the correlation coefficient between model and observations, "RMSE" is the root mean square error. Different color dots represent different regions as shown in Fig. 6.

990

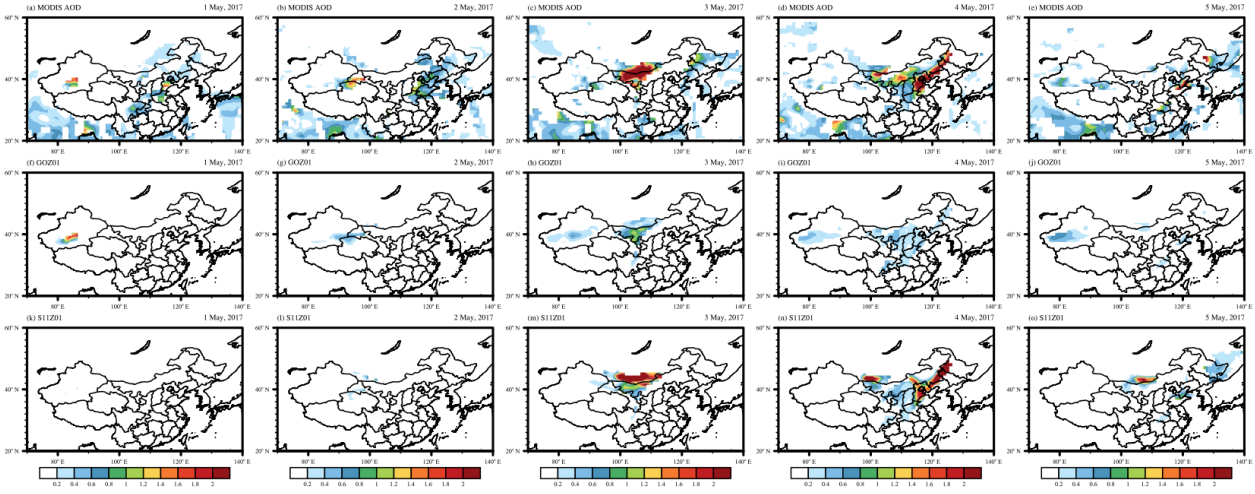

Figure 9. Simulated and observed **mean** AOD ~~on 4 May, 2017~~**over the simulation period 1-5**~~7~~ **May. Panels (a)(b)(c)(d)(e) show the distribution of** ~~: (a) Distribution of~~ daily mean aerosol optical depth (AOD) at 550 nm derived from MODIS-Aqua**. Panels (f) (g) (h) (i) (j) show the** ~~;~~ WRF-Chem simulated AOD ~~at 13:00 p.m. local time~~ for ~~six experiments (b)~~ GOBS95 **experiment. Panels (k)(i)(l)(m)(n) show the WRF-Chem simulated AOD for S11Z01 experiment. The model results are extracted from the simulation results at 13:00 local time for each region to match the MODSI observation time (details see Sect. 2.5). All the other experiments and for the period 1-6 May are shown in the supplementary (Fig. S1).** ~~, (c) GOPE92, (d)GOZ01, (e)S11BS95, (f)S11PE92, (g) S11Z01.~~ **Grid points without valid MODIS AOD retrieval are masked for both observational and model results.** ~~The simulated AOD already collocated with MODIS AOD.~~

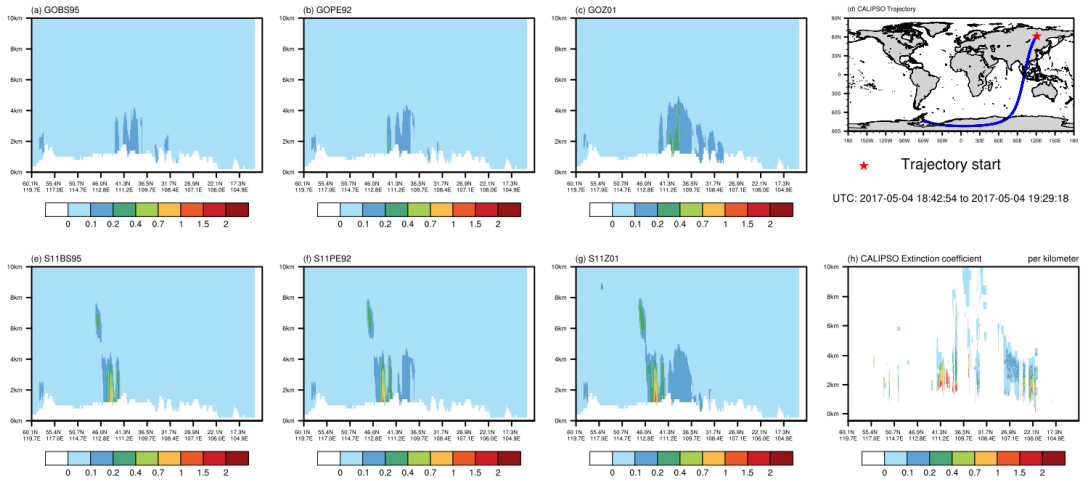

Figure 10. Simulated and observed aerosol extinction profiles at 532 nm at 18:00 UTC 4 May. Panel (d) show the CALIPSO trajectory. Panel (h) show the CALIPSO observed extinction coefficient. Panels (a)(b)(c)(e)(f)(g) show the WRF-Chem simulated extinction coefficient from six experiments.

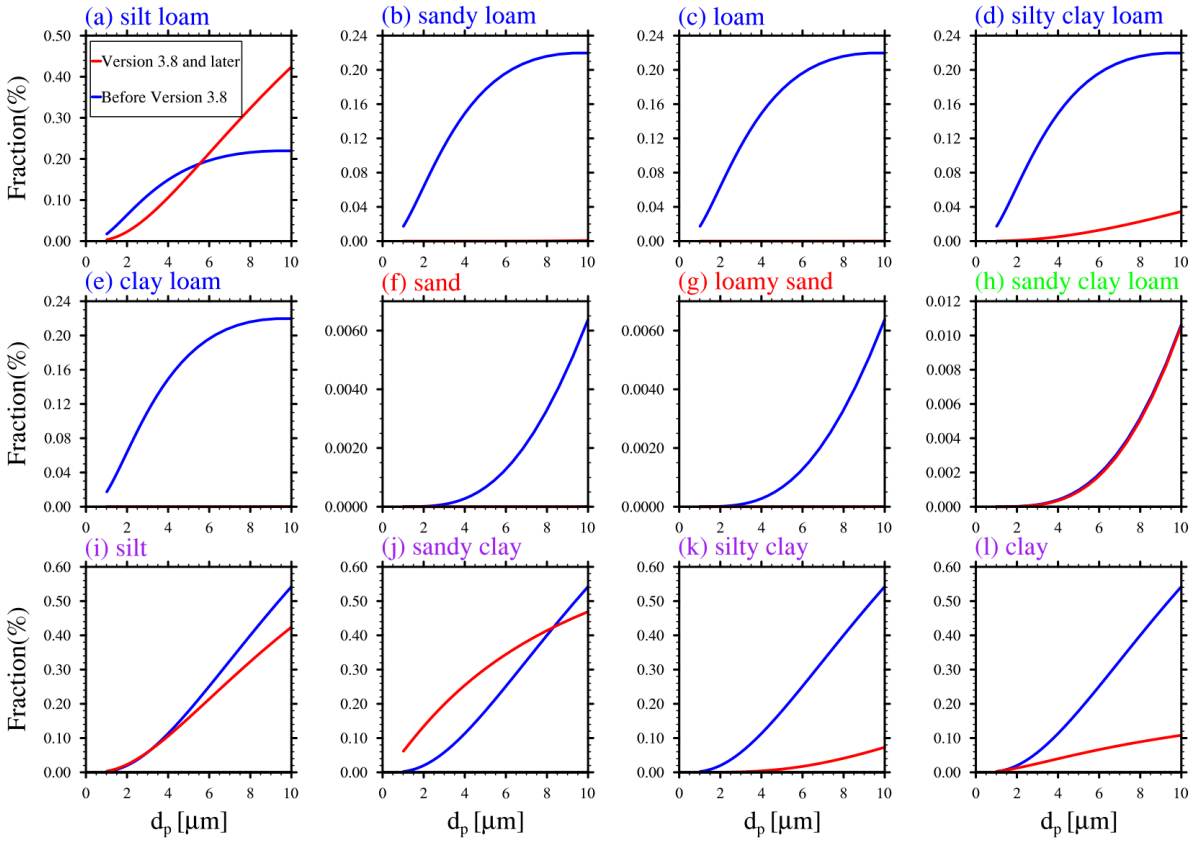

Figure B1. Free dust fraction for 12 soil types as a function of particle diameter (~~Dp~~**d**). The red lines represent the free dust fraction in WRF-Chem v3.8 and later versions. The blue lines represent the free dust fraction before WRF-Chem v3.8. The colors of the soil type font in the upper left corner of the plot are different. In WRF-Chem v3.8 and later versions, each soil type has a corresponding free dust fraction distribution. In versions before WRF-Chem v3.8, several soil types share a free dust fraction distribution. The same soil type font color indicates that a free dust fraction is shared among these soil types in versions before WRF-Chem v3.8.